Red Mud resources for metal

Subjects: Materials Science, Ceramics

Contributor: Sneha Samal

Various scopes are suggested for the utilization of red mud to maintain a sustainable environment. The potential use of red mud covers the valuable metal recovery that could emphasize the use of red mud as a resource. Red mud could act as reduced slag in the metallurgical field for the extraction of minerals and metals for upscale application. Although many studies have revealed the potential utilization of red mud, most of them are only limited to a lab-scale basis.

Keywords: red mud ; resources ; reduced slag ; metal ion recovery ; mineralogical

1. Introduction

Red mud is one of the by-products generated in the aluminum industry from the ore of bauxite during the calcination process for the extraction of aluminum dioxide. The term “red mud” is established and derived from the two words of “red”, which refers to the color, and “mud”, which refers to the waste generated after the alumina extraction from the bauxite ore, by a calcination process. Generally, 2.5–3 kg of red mud is produced in each 1 kg of Al production from the bauxite industry . As the global production of aluminum is approximately 64 million tons, this result in 160 million tons of red mud to dispose of. The current method of red mud disposal is to simply pump it into ponds or dry up the red mud with a special liner [1]. In both approaches, a large amount of land is used and ultimately the land should be maintained properly, rather than disposing of the product as waste to the surrounding area, causing serious environmental issues and health hazards. The alkaline nature of red mud and dried-up dust disposable to the environment could be minimized by spraying water on the dry red mud powders. Furthermore, the alkaline nature of red mud inhibits the vegetation growth in those areas, thus it must be corrected by adding acidic flux before its disposal into the surroundings. Given all these environmental implications, it would be appropriate to think of a new use for red mud. “Waste is a resource if we use it. Otherwise, it is waste if we waste it” [1]. Thus, the red mud residue, after the extraction of the minerals, could be considered as a potential building material for the construction of roads, landfill sites, and building materials. Recently, a combination of red mud–fly ash composite could find application in the preparation of geopolymers as an alternative material for the construction industry [2].

The recovery of critical raw materials from red mud involves many benefits including environmental, social, financial, economic, and technological benefits [2][3]. The content of metals such as Ti, Si, Fe, Na, and Al in red mud is 2–12%, 1–9%, 14–45%, 1–6% and 5–14% respectively. Apart from representing a huge solution in the construction sector, when present in a large quantity, red mud as a resource opens up various possibilities for the extraction of minerals and ions such as the major elements Fe, Ti, Mn, Al and Ca, Na, Si, Cr, Mn, V, La, Sc, Y. Rare earth elements (REE) such as Ce (102 mg/kg), La (56 mg/kg), Sc (47 mg/kg), Nd (45 mg/kg), Sm (9 mg/kg) are also valuable elements present inside red mud. REE are the most important critical raw materials for the European Union [4]. Red mud can be also considered as sintered ceramics for electroceramic materials [5][6][7].

In powder technology, red mud could be considered as resource for the recovery of metals such as Fe, Ti, Mn, Na, K [8][9]. Simultaneously, red mud could be used as a coating material for various composites against harsh environments and high-temperature sintering, against wear and corrosive behavior [10][11][12]. Unlike the recovery of metal ions, which will certainly not be the main business for the red mud, it could also act as the main component for construction and road fill materials [13][14]. Fly ash with acidic nature inhibits agglomeration of the volatilization of heavy metals at low temperatures within the red mud combination [15][16][17].

In Figure 1 the combination of various technologies that could be implemented for a complete utilization strategy is shown. The comprehensive utilization of red mud as a resource opens up in various sectors such as red mud-based geopolymers in the construction and metal extraction industries. Synergetic utilization of red mud emerges as flue gas in the geopolymer industry sector for an alternative binder in cement material. The exploitation of these potential techniques, for metal extraction from red mud, is subordinate to the establishment of a small plant, near the aluminum industry, for resource utilization [18][19][20][21]. The reduction of red mud and fly ash mixtures proved the formation of reduced slag in the

sintering process during lab-scale experiments. Based on the latter, it is possible to design a synergetic utilization for the red mud/fly ash mixture. It has been seen that the hazardous heavy metals could be recovered as alloy from the reduced slag [22][23]. Therefore, this environmentally friendly co-reduction process could be implemented as one sound solution for red mud and fly ash, leading to complete utilization of the resources, thus representing a zero-waste technology [24]. The optimized parameters for the reduction process were chosen as 20 wt.% fly ash with 80 wt.% red mud, at a temperature of 1100 °C for 2 h. The sintered slag contained CaO, SiO_2, Al_2O_3, and FeO, as well as a glass phase, which is similar to ground-granulated blast-furnace slag and supports broad future applications. It has also been seen that the treatment of the red mud's alkaline nature with an additive for surface modification will enhance the utilization on an upscale basis [25] [26]. The major and minor elements of red mud are quantified in Table 1.

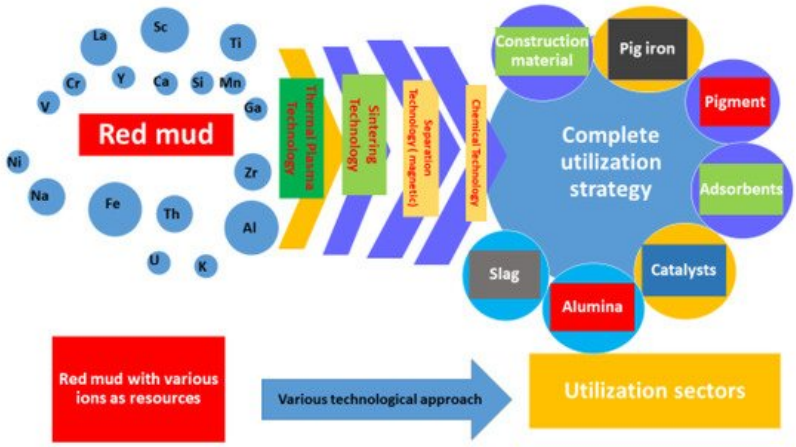

Figure 1. Scheme representing the technologies implemented in red mud for its complete utilization in various sectors.

Table 1. Quantification of major elements (wt.%) and minor elements (Conc. Mg/kg) of red mud.

Red Mud Compositions				
Major Elements	**Wt.%**	**Minor Elements**	**Concentration (mg/kg)**	**Refs.**
Fe_2O_3	30–60	U	50–60	[27]
Al_2O_3	10–20	Ga	60–80	[28][29]
SiO_2	3–50	V	730	[28][29][30][31]
Na_2O	2–10	Zr	1230	[32][33]
CaO	2–8	Sc	60–120	[34]
TiO_2	8.50	Cr	497	[34]
P_2O_5	0.25	Mn	85	[35]
MgO	0.10	Y	60–150	[35][36]
K_2O	0.06	Ni	31	[34]
–	–	Zn	20	[34]
–	–	La	0.1–1%	[37]
–	–	Th	20–30	[38]

The composition shows the presence of heavy irons and minerals of Fe, Si, and Ti in the major quantity. Red mud could be considered as bricks, road surface material, and in the cement industry with potential use for building applications. However, this approach is limited due to the alkaline nature of the material. The alkaline nature of red mud is reduced by the acidic counterpart of fly ash, generating the neutral nature of the composite. The latter could be the most significant solution for the vastness of the problem, but careful consideration is required for this application. After the Al content, Fe represents the second-largest amount of metal that is separated by a magnetic separator. The nonmagnetic part of the residue can be considered as a construction material. Furthermore, some researchers searched for producing steel and cement from red mud [39]. Additionally, the recovery of Al, caustic soda, and lime could be used as catalyst for enhancing the Bayer process for increased Al production. However, despite the invaluable outcomes obtained from all techniques associated with red mud utilization, they are not practically suitable to use for recycling large amounts of red mud

(currently 160 million tons annually [40]). The amount or iron in red mud is the largest, which, when disposed with red mud annually, represents a waste of metal [41]. Thus, metal recovery from red mud opens a wide field for potential utilization as resource.

2. Sources and Utilization of Red Mud

2.1. Relevant Sources for Literature Review

A broad range of literature sources, dating from 1991 to 2021, in the areas of red mud and red mud composites were reviewed for this article. The databases searched for this literature survey include various sources such as MDPI, Scopus, Science Direct, Google Scholar, and Springer. Articles, conference proceedings, data, reviews, chapters, and books of similar topics were filtered using search terms such as “red mud”, “composite”, “mineral”, “microstructure evolution”, “metal ion recovery”, “mineralogical characteristics of the materials”. Section 1 in the introduction includes all the potential previous studies in this area. Section 2 includes various types of red mud and composites with potential applications. The basic and advanced application of red mud and composite is followed in Section 3 with emphasis on some recent literature surveys. Section 4 compares the data with the present scenario through an exhaustive literature survey. Figure 2 displays the total publication from 2010–2021 in the area of red mud that consider it as a source of metal and ions.

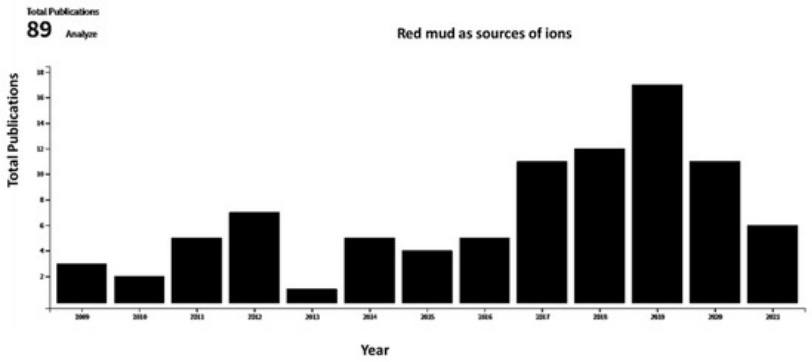

Figure 2. Total publications as function of year for red mud considered as source of ions (data collected from Web of Science).

2.2. Utilization of Red Mud as Metal Resource

Although researchers highlight that red mud is a large contributor to the construction sector, it is generally recognized as waste material. The term “waste” creates, both psychologically and from a media viewpoint, an obstacle in the application areas. Thus, replacing the term “waste” with “resource” could add significant interest in the extraction of minerals and their use. In this work, an investigation was carried out for review in the area of utilization of red mud as a source of metallic ions and resource material. Red mud, added with various weight percentages of fly ash to neutralize the acidity, undergoes the sintering process for the conversion into a reduced slag material. This sintered product could act as a basic resource for the extraction of metal ions and as a major by-product for the mineral industry. Figure 3 illustrates the red mud utilization from the as-received stage towards the final stage for industrial utilization.

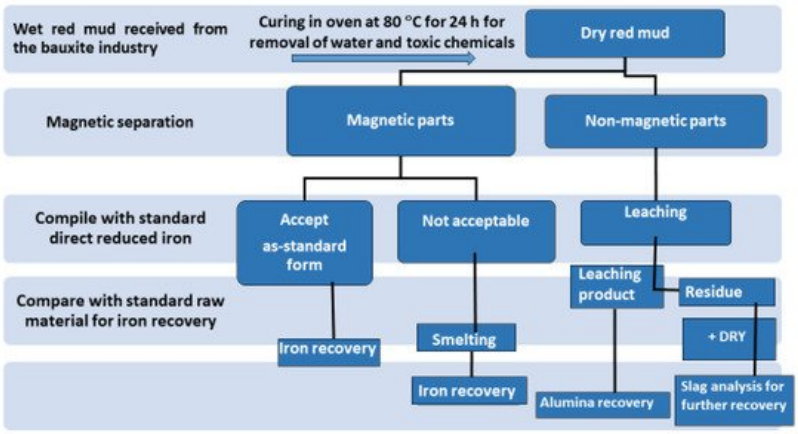

Figure 3. Schematic flow sheet on the iron, alumina, and slag for recovery of various metals.

The dry red mud undergoes magnetic and non-magnetic separation that follows up the smelting process for iron recovery. Non-magnetic parts undergo the leaching process for Al recovery. Figure 3 portrays the flow sheet of various types of red

mud utilization. Preliminary treatment involves the magnetic separations of bulk iron parts from the red mud. Accordingly, the magnetic and non-magnetic parts undergo different treatment in the further steps for iron recovery on the acceptable norms. If the magnetic parts are non-acceptable, they undergo smelting for iron recovery. The non-magnetic parts undergo leaching for alumina recovery and the residue undergoes slag recovery as the utilization of the major parts. A key point to benefit in terms of human resources and the economy could be the establishment of a plant for the beneficiation of red mud as resource alongside the bauxite industry. Particularly, to avoid transportation costs, the waste utilization facility processes and tools such as electric arc furnace, sintering of red mud, and leaching facility should be present in the proximal areas of the aluminum industry. One of the innovative processes in the production of pig iron is a by-product from reduced red mud by the carbothermal reduction process. The various process and active areas in which red mud can be treated can be divided into major and minor activities (Figure 4). Red mud can be used as a primary resource in the construction industry, for example, as bricks and other suitable materials for making houses, or as material for pavement. Red mud could be used in the industrial sector of iron recovery or metal extraction and smelting for the by-product of pig iron and calcium titanium-rich compounds for recovery of titanium. Finally, it can be used in the carbothermal reduction process for iron recovery, which could be a possible step for steel making. The rest of the residual red mud could be considered as the reductant for alumina recovery. Major use in the areas of construction and landfill opens the application of red mud in combination with metal recoveries such as Al, Fe, and its integrated combination towards the reduction process for the steelmaking. Integrating the red mud with other materials could improve its use in synergetic utilization [41].

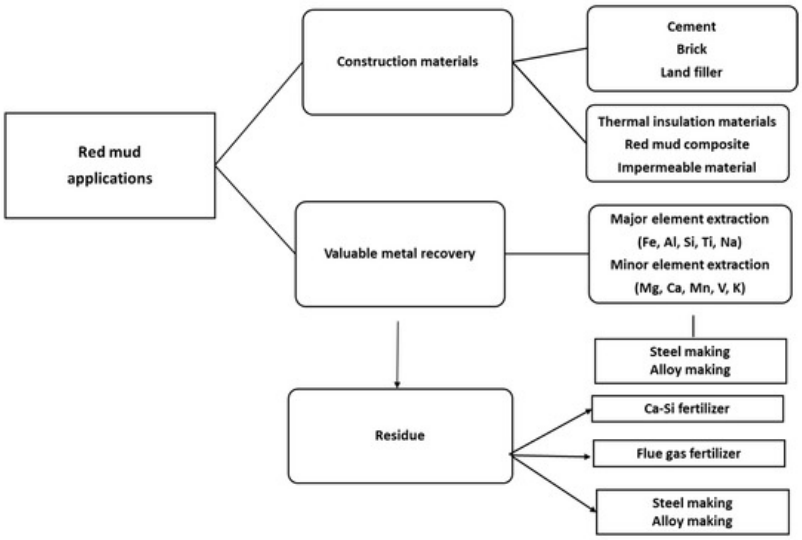

Figure 4. The various areas of red mud utilizations.

Foaming ceramics are emerging as a new group of materials that could improve performance that could act as energy-saving materials [42]. Sintering and thermal plasma open the possibility of the synthesis of energy-saving materials by generating porosity in the sintered material [43][44]. In these cases, sintering is one of the effective processes of using carbo-thermal reduction inside the furnace that facilitates the formation of sintered slag. The quantity of fly ash content (wt.%) reduces the mixture of red mud and fly ash that undergoes chemical and physical reduction processes as a function of sintering temperature. The mineralogical evolution in the sintered product and the end-product was examined to confirm the presence of minerals and ions at the end of the process.

2.3. Sources of Metal Ions

In this article, an effort was made to create a review in the area of utilization of red mud as a source of metal ions. Various steps and process related to the mineralogical evolution of various metal and rare earth ions in red mud are covered and discussed. Simultaneously, the application of red mud in various fields is covered, where red mud could be given importance as a resource rather than waste.

Table 2 shows the red mud generated from various plants with different chemical compositions.

Table 2. Major elemental composition of red mud from various locations in the countries.

Composition wt.%														
Location	Al_2O_3	Fe_2O_3	SiO_2	TiO_2	CaO	Na_2O	Mn	P_2O_5	V_2O_5	Gd_2O_3	MgO	K_2O	LOI	REFs
Ajka Aluminum Industry, Hungary	16–18	33–48	9–15	4–6	0.5–3.5	8–12	-	-	0.2–0.3	-	0.3–1	-	-	[31]
Aluminium Pechiney, Gardanne, France	15.00	26.62	4.98	15.76	22.21	1.02	-	--	-	-	0.95	-	12.10	[33]
Bauxite ore refinery, Guinea	26.60	48.40	5.50	-	1.30	-	-	-	-	-	0.90	-	14.60	[32]
ALCOA factory, San Cibrao (Northwest of Spain)	12.00	37.00	9.00	20.00	6.00	5.00	-	-	-	-	-	-	-	[35]
Korea Chemical Co.	23.70	16.60	22.90	6.70	6.70	11.60	-	-	-	-	-	-	-	[36]
Shandong Aluminium Factory, China	7.96	6.57	21.90	-	38.84	2.32	-	-	-	-	1.60	0.41	17.42	[37]
Greek red mud, Greece	15.60	42.50	9.20	5.90	19.70	2.40	-	-	-	-	-	-	-	[38]
Slurry pond from Worsley Alumina, Australia	15.00	60.00	5.00	5.00	-	16.00	-	-	-	-	-	-	-	[39]
Alpart factory and the Alcan Ewartonred mud pond, Jamaica	18.80	45.30	4.30	6.40	3.10	1.50	-	-	-	-	-	-		[40]
Shandong Aluminium Corporation, Shandong, China	6.93	12.76	19.14	3.43	46.02	2.37	-	-	-	-	1.15	1.20	5.73	[41]
Alumina-aluminio of San Ciprian, Lugo, Spain	20.10	31.80	6.10	22.60	4.78	4.70	-	-	-	-	0.20	0.03		[42]
Etibank Seydiehir Aluminium Plant, Konya, Turkey	20.39	36.94	15.74	4.98	2.23	10.10	-	-	0.05	-	-		8.19	[43]
Aluminium of Greece S.A.	15.65	45.58	6.96	7.07	14.84	3.26	-	-	-	-	-	0.07	-	[44]
Eurallumina alumina plant, Italy	17.19	30.45	9.58	8.61	7.77	12.06	-	-	-	-	0.86	0.30	12.38	[45]
Queensland Alumina Ltd. refinery, Gladstone, Australia	25.45	34.05	17.06	4.90	3.69	2.74	-	-	-	-	1.86	0.20	-	[46]
Seydiehir Aluminium Plant, Konya, Turkey	14.10	38.30	2.50	-	4.10	-	-	-	-	-	-	-		[47]

Composition wt.%														
Location	**Al_2O_3**	**Fe_2O_3**	**SiO_2**	**TiO_2**	**CaO**	**Na_2O**	**Mn**	**P_2O_5**	**V_2O_5**	**Gd_2O_3**	**MgO**	**K_2O**	**LOI**	**REFs**
HINDALCO Renukoot, India	**21.9**	**28.1**	**7.5**	**15.6**	**10.2**	**4.5**	**–**	**–**	**–**	**–**	**-**	**-**	**12.2**	[48]
IND ALMuri, India	**24.3**	**24.5**	**6.2**	**18.0**	**–**	**5.3**	**–**	**–**	**–**	**–**	**-**	**-**	**–**	[48]
BALCO Kobra, India	**19.4**	**27.9**	**7.3**	**16.4**	**11.8**	**3.3**	**–**	**–**	**–**	**–**	**-**	**-**	**12.6**	[48]
NALCo Damanjodi, India	**14.8**	**54.8**	**6.4**	**3.7**	**2.5**	**4.8**	**1.1**	**0.67**	**0.38**	**0.01**	**-**	**-**	**9.5**	[48]
INDALBelgam, India	**19.2**	**44.5**	**7.0**	**13.5**	**0.8**	**4.0**	**–**	**–**	**–**	**–**	**--**	**-**	**10.0**	[48]
MALCO Mettur Dam, India	**14.0**	**18.0**	**56.0**	**50.0**	**2.0–4.0**	**6.0–9.0**	**–**	**1.0–2.0**	**–**	**–**	**-**	**-**	**12.60**	[48]

3. Physical and Chemical Properties of Red Mud

3.1. Particle Size Distribution and pH of Red Mud

Red mud, generated as waste in the aluminum industry and generally disposed of in the surrounding areas, was supplied from an Indian bauxite producer (Bharat Aluminium Company Ltd., BALCO, Korba, Chhattisgarh, India). Fly ash was supplied from the thermal power plant (Coal Plant, India). The slurry red mud received directly from the aluminum industry contains a lot of water and moisture. Red mud needs to be dried at 100 °C for 24 h, to remove the water and chemicals such as volatile compounds in a standard furnace in an air medium. The particle sizes of the red mud and pH change as a function of time, as shown in **Figure 5** [49].

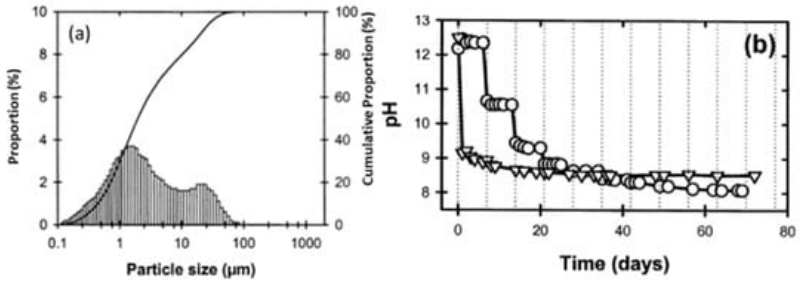

Figure 5. (**a**) Particle size distribution versus cumulative proportion in red mud as the residue from the alumina industry; (**b**) pH as a function of time. Reprint with permission from ref. [49]. Copyright 2004, Wiley.

Red mud consists of various fine-size particles within the range of 0.1–100 µm. Average particles fall within the range of 1 µm. The alkaline nature of red mud decreases as the function of the day, from fresh red mud to aged, and becomes stable. Red mud was mixed with fly ash contents from 0 to 20 Vol% to observe the effect of neutralization of alkaline components with acidic flux by using agate mortar.

3.2. Ternary Phase Diagram of the $CaO–Al_2O_3–SiO_2$ System

Observation of the mineral compounds in the system of the $CaO–Al_2O_3–SiO_2$ phase diagram reveals the red mud–fly ash falling into the category (**Figure 6**).

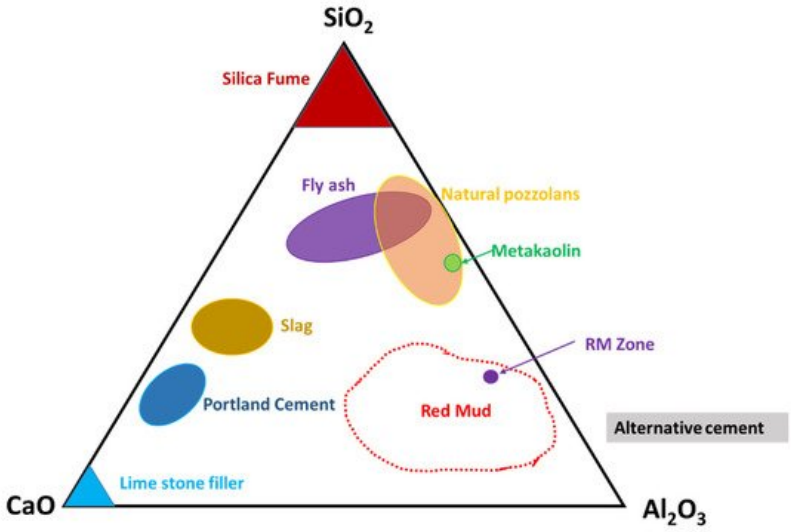

Figure 6. Ternary phase diagram of the $CaO–SiO_2–Al_2O_3$ system that covers red mud and fly ash zones. Reprint with permission from ref. [50]. Copyright 2013, Elsevier.

Thus, their presence in such a diagram could open up the possibility of mixtures of red mud and fly ash for utilization as an alternative cement category for construction purposes. The mixture falls within the zone of slag that could be boosted as a source of metal extraction as well and act as compatible material for alternative cement in the construction industry.

3.3. Phase Transformation during Thermal Decomposition

Differential thermal analysis of red mud showed the combined effect of the decomposition reaction, concerning the weight loss and the associated energy changes. **Figure 7** shows the evolution of red mud as the function of temperature concerning exo- and endothermic reactions [49].

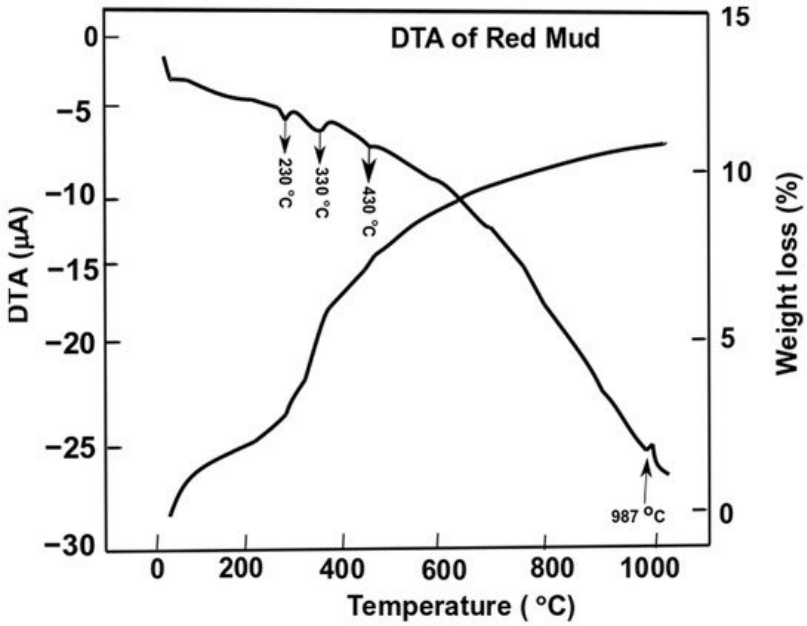

Figure 7. Differential thermal analysis of red mud with peak evolution and weight loss as a function of the temperature. Reprint with permission from ref. [51]. Copyright 2015, Elsevier.

Gibbsite phase emerges between 320 and 330 °C whichderives from the decomposition of $x\text{-}Al_2O_3$. The decomposition reaction of goethite FeO(OH) into hematite and water occurs as follows:

$2\alpha\text{-}FeO(OH)\ (s) \rightarrow Fe_2O_3(s) + H_2O\ (g)$

(1)

whilst the gibbsite decomposes into boehmite and x-alumina in the range of 230–330 °C

$Al(OH)_3\ (s) \rightarrow AlO(OH)\ (s) \uparrow (\text{water evaporates})$

(2)

$2AlO(OH)\ (s) \rightarrow Al_2O_3(s) \uparrow$ (water evaporates)

(3)

Furthermore, goethite continues to decompose into hematite at 440 °C,
$3\ Fe_2O_3\ (s) \rightarrow 2Fe_3O_4\ (s) + ½O_2\ (g)$

(4)

The alumina phase of red mud is very stable until higher temperatures. In the range of 900–1100 °C the formation of nepheline from cancrinite occurs
$3CaO\ (s) + Al_2O_3\ (s) \rightarrow Ca_3Al_2O_6\ (s)$

(5)

and further decomposition reactions happen above 1100 °C
$Fe_2O_3\ (s) \rightarrow 2FeO\ (s) + ½O_2\ (g)$

(6)

$2FeO\ (s) + TiO_2\ (s) \rightarrow Fe_2TiO_4\ (s)$

(7)

$3CaO\ (s) + Fe_2O_3\ (s) + 3\ SiO_2\ (s) \rightarrow Ca_3Fe_2Si_3O_{12}\ (s)$

(8)

$7Ca_3Al_2O_6\ (s) \rightarrow Ca_{12}Al_{14}O_{33}\ (s) + 9CaO\ (s)$

(9)

$Ca_3Al_2O_6\ (s) + Na_2O\ (s) \rightarrow Na_{2x}Ca_{3-x}Al_2O_6\ (s) + xCaO\ (s)$

(10)

The weight loss of the sample of red mud is observed significantly towards higher temperatures. At 1000 °C, there is significant weight loss and more than 10 wt.% loss is observed. DTA analysis reveals the behavior of red mud sintered at a higher temperature.

3.4. Microstructure of Sintered Compound at 1100 °C Temperature

The sintering process further facilitates the mixture as the form of the pellet. Cylindrical pellets were prepared with a dimension of 0.5 × 2.5 cm^2 by using water as a binder at a pressure of 50 MPa. The pellet of red mud–fly ash mixtures with various contents undergoes co-reduction in the graphite resistance furnace for sintering at various temperatures, 1000–1050–1100 °C, for a duration of 2 h in a static argon atmosphere, followed by cooling (2 h).

In **Figure 6**, the microstructure evolution of as-received red mud in dry condition and sintered samples are presented. Globular particles, with fine size in a range from a few microns to the maximum particle size of 100 µm, are displayed (**Figure 8**a). The sintered composite of red mud-fly ash at the various wt.% shows the evolution of various phases as the function of temperature (**Figure 8**b–d). Iron phases of magnetite are shown in a lighter color and the darker region belongs to the quartz. Whereas, sintered red mud–fly ash composite shows isolated pores, elongated shape, and size of the crystals and ceramic matrix with some former phases. The sintered sample with 20 wt.% of fly ash shows that the porosity in sintered composite increased with irregular (Fe_3O_4), goethite (FeO(OH)), iron (Fe), hercynite ($FeAl_2O_4$), and aluminum silicates. Additionally, 20 wt.% of fly ash and sintering at various temperatures allows conversion of complex phases towards simpler phases of compounds of magnetite, iron, calcium aluminosilicate, sodium aluminum silicates, and Goethite phases [51][52].

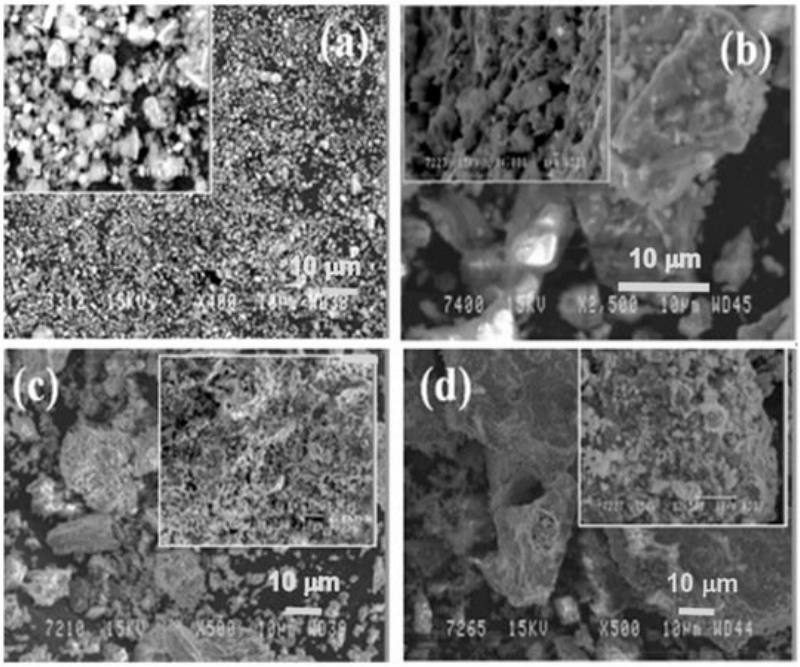

Figure 8. (**a**) Surface features of the red mud at RT; (**b**) sintered red mud without fly ash content; (**c**) sintered red mud with 10 wt.% of fly ash content; (**d**) sintered red mud with 20 wt.% of fly ash content at 1100 °C sintered temperature. Reprint with permission from ref. [51]. Copyright 2015, Elsevier.

3.5. Phase Evolution of Sintered Sample as a Function of Temperature

Figure 9 displays the various phases of magnetite, calcium aluminum silicate, sodium aluminum silicate, goethite, iron, and perovskite as a function of sintering temperature. The phases show a trending behavior with fly ash mixtures of 10 wt.% (**Figure 9**a,b). On increasing the percentage of fly ash content (up to 20 wt.%) phase evolution is more stable and distinct (**Figure 9**c). Metal ions into the various phases are more prominent at lower sintering temperatures without the addition of fly ash [53][54][55]. However, the phases are more distinct and accurate with more specific phases of simpler compounds at a higher sintering temperature of 1100 °C with 20 wt.% of fly ash content. The reduced sintered slag contains various metal ions and mineral sources for the recovery of metal and ions for further utilization in industry [56][57][58].

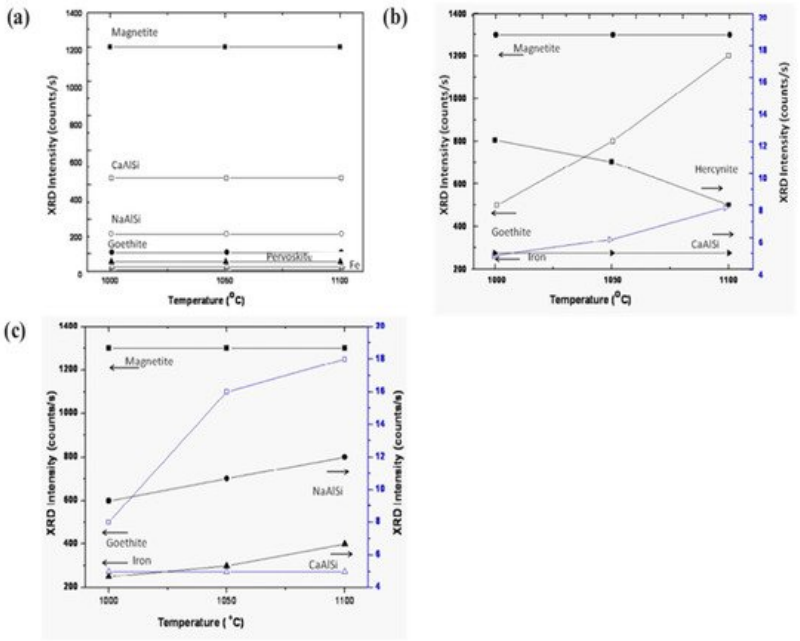

Figure 9. Evolution of various compounds as the function of sintering temperature: (**a**) sintered red mud without any additives; (**b**) sintered red mud with 10 wt.% of fly ash content; (**c**) sintered red mud + 20 wt.% fly ash mixture. Reprint with permission from ref. [51]. Copyright 2015, Elsevier.

3.6. Carbo-Thermal Smelting Technology

Carbo-thermal reduction of bauxite is developing as a promising alternative technology for the aluminum and aluminum alloy industries. In this process, carbon or coke are used as a reductant for solid-state reduction technology. As a result, metallic iron, ferroalloy of silicon and aluminum, titanium carbides could be obtained as the by-products [15][16]. Based on the smelting technology, we performed previous work on using fly ash additive with the red mud that undergoes sintering technology for the building materials. A combination of smelting and reduction processes allows a reduction in the temperature of 1200–1500 °C to produce slag phase and cast iron if the C content in the cast iron is within the range of 2–2.3%. Another direct route for separation of iron from red mud is the roasting method followed by magnetic separation. Iron (Fe) could be separated from red mud using various methods, either by leaching or by sintering or roasting. As one of the major elements, Fe should be extracted from red mud following various reaction, as outlined below [59][60][61].

Fe_2O_3 (s) + C (s) → Fe_3O_4 (s) + CO (g)

(11)

Fe_2O_3 (s) + 3C (s) → Fe (s) + 3CO (g)

(12)

CO_2 (g) + C (s) → 2CO (g)

(13)

$3Fe_2O_3$ (s) + CO (g) → $2Fe_3O_4$ (s) + CO_2 (g)

(14)

Fe_3O_4 (s) + CO (g) → 3FeO (s) + CO_2 (g)

(15)

FeO (s) + CO (g) → Fe (s) + CO_2 (g)

(16)

FeO (s) + C(s) → Fe (s) + CO (g)

(17)

The phases were more prominent in the reduced sample of red mud when 20 wt.% of fly ash was used, which is shown in the SEM images reported in **Figure 10**.

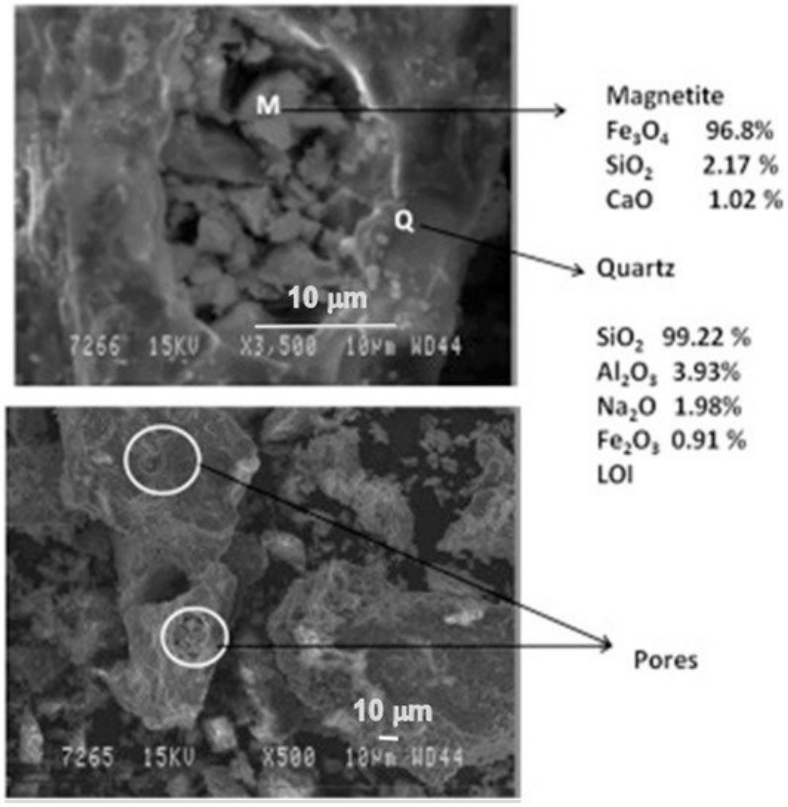

Figure 10. Micrograph of the sintered red mud with 20 wt.% of fly ash content in 1100 °C sintered temperature. Reprint with permission from ref. [51]. Copyright 2015, Elsevier.

The evolution of the different phases developed in the reduced sample sintered up to 1100 °C was recorded with the XRD technique and is shown in **Figure 11**.

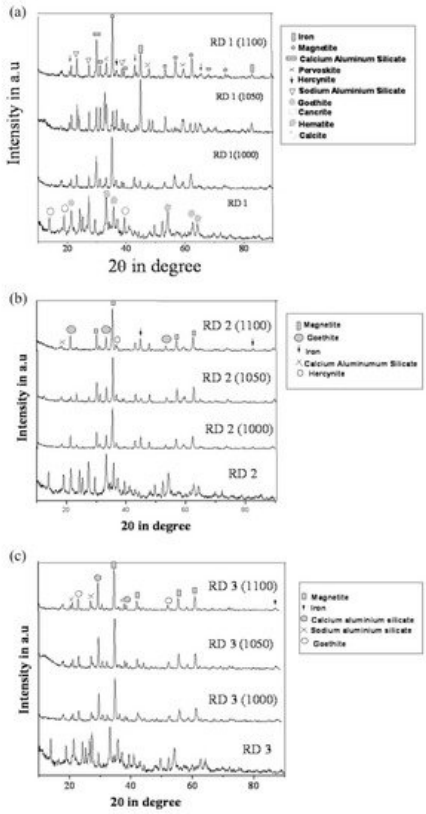

Figure 11. (**a**) Diffraction profile of red mud and sintered red mud at various temperatures; (**b**) diffraction profile of red mud and sintered red mud with 10 wt.% fly ash; and (**c**) diffraction profile of red mud and sintered red mud with 20 wt.% of fly ash content. Reprint with permission from ref. [51]. Copyright 2015, Elsevier.

Iron is the major element in red mud that could directly reduce the carbon-bearing pellets of red mud with coal at a temperature of 1400 °C for 30 min [62]. The obtained products contain 96.52% iron with low Mn and Si contents. However, P and S contents are high.

4. Fields of Application of Red Mud

A considerable environmental concern associated with red mud is associated with its high pH value and its small amounts of heavy metals. These days, the aluminum industries are more focused on producing a cleaner residue from bauxite.

4.1. Thermal Plasma Technology for the Production of By-Products from Red Mud

The thermal plasma technology boom, as a prospective area of waste management, is widely reported in the literature and could be used as a technology to reduce the amount of red mud to produce pig iron [63][64][65]. Red mud mixed with carbon graphite undergoes a smelting process to produce pig iron with 71% recovery. This process allows for reduced energy consumption with recovery of metals from the red mud. Waste treatment is considered one of the efficient methods in the energy sector and thermal power plants. Simultaneously, pig iron could be extracted from red mud by adding a fluxing agent of graphite and fluxes [66][67][68].

4.2. Mixing Technology for Use of Red Mud as an Additive for Construction Materials

Mixing technology is a methodological way of approaching red mud as an alternative replacement of cement. Partially, red mud can be used in slag for the cementitious material that can be used effectively in building sectors [69][70][71]. Red mud is also considered to add a neutralization effect of the hydration properties of cement materials in the construction industry. Bricks and prisms are some of the resources that could be derived from the red-mud-based geopolymer matrix in areas of the building sector. Red mud is considered as environmentally friendly, self-sensing concrete blended with by-product waste. Red mud is also considered as one of the potential additives for durability and mechanical performance of cement mortars. Geopolymerization of red mud and the slag from ferronickel could emerge as advanced inorganic polymeric material with exceptional physical and chemical properties [72][73].

4.3. Separation and Extraction Technology

The separation of the magnetic materials from red mud is considered to be the preliminary step for the separation of iron particles. Simultaneously, extraction technology is more effective in leaching such as chemical technology for the separation of various minerals. The leaching of red mud or sintered red mud is very effective in various sectors for the adsorbents and catalyst categories [74][75][76]. The red mud–fly ash mixtures could be considered as a sustainable acid mine drainage management system. Slag and cement mortar containing non thermally treated dried red mud is considered as opening demand for potential utilization. Red mud is considered an effective additive in geopolymer materials for the adsorption of heavy metal ions.

4.4. Coating Technology

Coating technology opens the door for applications in pigment areas using Ti as pigment ion. Red mud could be used as a coating by thermal plasma spray technologies for wear resistance coating or corrosive resistance coating layers that could stand as a barrier against environmental conditions [77][78][79]. Coatings based on red mud offer an important erosion wear resistance, which can further be improved. Red mud could act as deposition material for surface modification technologies in the plating, diffusion process, surface hardening, and thin-film coating sectors. The red mud–polyester composite coating could act as neutron shielding materials from injurious effects of radiation [80][81][82], thus representing an innovative application of red mud in the industrial sector.

Red mud has emerged as a significant contribution to the hybrid composite. Red mud can be used as a resource for transferring a waste-management approach with natural fibers. A hybrid composite concept has been developed for the potential in a red-mud-based geopolymer matrix with the incorporation of fibers [83].

4.5. Economic and Social Impact

The potential application of red mud in the various industrial sectors proves that valuable resources will have a significant impact on the economic prospects, boosting economic growth through its potential as a valuable by-product. The social impact will increase only by using it as a resource rather than dumping as waste that holds a threat for environmental pollution [84][85][86]. The significant use of red mud as a resource will reduce the risk of environmental hazards and socially benefit environmental conditions.

4.6. Value Recovery and Strategic Utilization

The valuable elements in red mud can be recovered by acid leaching, solid-state carbo-thermic reduction, magnetic and fluidized bed separation, as well as smelting in a blast furnace. In the framework of considering red mud as a resource, we need to improve various steps of metal recovery as one of the potential applications for the pigment industries.

The elemental composition and its derivation from red mud, bauxite residue, and their respective Raman spectra for various elements are shown in **Figure 12** [87]. A red mud image scan analysis shows minerals and ions present in the sample (**Figure 12**) [88].

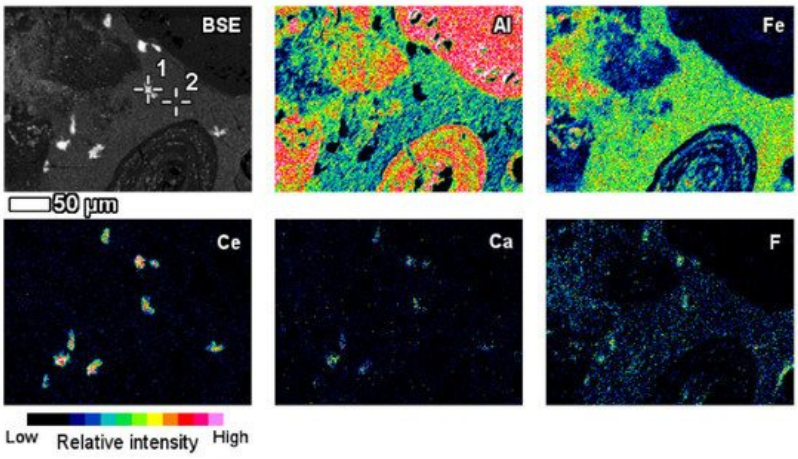

Figure 12. Backscattered image of red mud and elemental image analysis for various elements of Al, Fe, Ce, Ca, F. Reprinted from ref. [87].

An insight investigation was carried out on various phases of rare earth elements in red mud. This approach leads to a mineralogical insight view with output to improve the rare earth elements recovery process. The distinct rare earth element (REE) phases are also contained within the lateritic bauxite (**Figure 12**).

The REE mineral content includes aluminum, cerium, phosphorous, and then other REEs. Thus, REE phases can be identified as belonging to the florencite group. The compositional analysis of elements is done by EDS spectrum exhibiting a pronounced phosphorus X-ray peak of **Figure 13**.

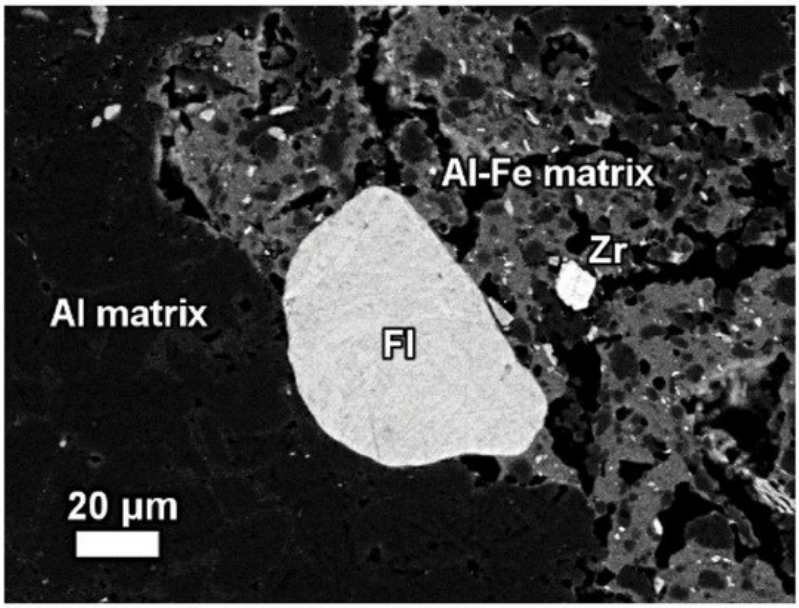

Figure 13. The mineralogical composition of red mud shows the presence of the florencite group of light rare earth elements, grain Zr grain, Al, matrix, and Al–Fe phase. Reprinted from ref. [87].

The composition of grains resembles rhabdophane–Ce which has been detected in the bauxite phase [89]. REE phosphate do not dissolve easily in sodium hydroxide which is generally used in the metal recovery process of bauxite.

LREEs are found as calcium containing phosphate phases in bauxite residue, more specifically as cerium phosphates (**Figure 14**a). It can be seen from the EDS spectrum of an analysed particle, exhibiting a pronounced phosphorus X-ray peak. A wide variation in chemical composition in morphological features is shown in **Figure 14**b.

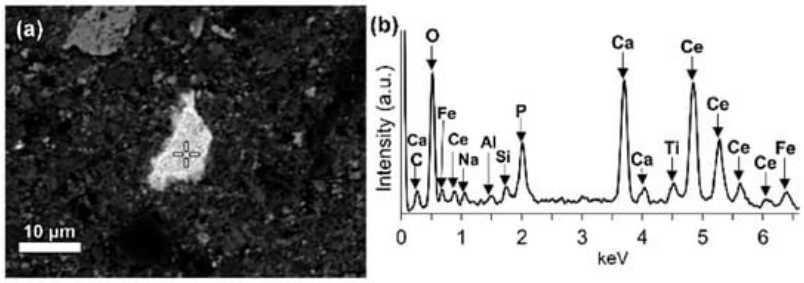

Figure 14. (**a**) Elemental composition of red mud shows the enlarged area of cerium phosphate and (**b**) its respective EDS spectrum. Reprinted from ref. [88].

Some LREE particles contain minor percentages of iron, titanium, and sodium oxide content (**Figure 15**a). The texture of ferrotitanate grains appears anhedral. Others showed distinct zonation expressed in wide variation in chemical composition as well as in morphological features. Most aggregates of anhedral globular crystallites can be observed on examining larger particles that exhibit a different reaction stage that has been observed in **Figure 15**b.

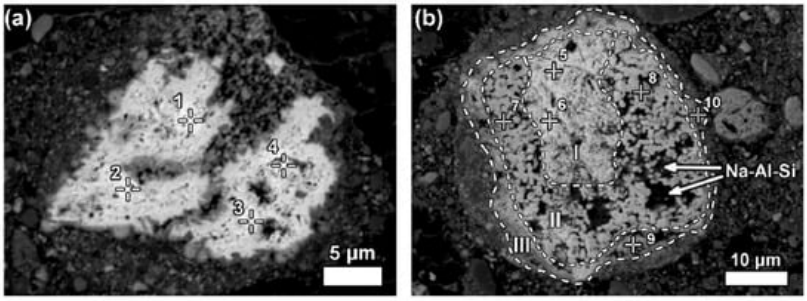

Figure 15. Neodymium–lanthanum as predominant LREE particles, of which (**a**) is partly reacted; and (**b**) exhibits a zonation (I–III) relating to reaction stages with Bayer liquor. Within zone II of (**b**), deposition of a sodium aluminosilicate phase (Na-Al-Si) is indicated. Reprinted from ref. [89].

The concentration of REE elements and major elements from red mud was investigated using ICP-OES and XRD elemental composition (**Figure 16**).

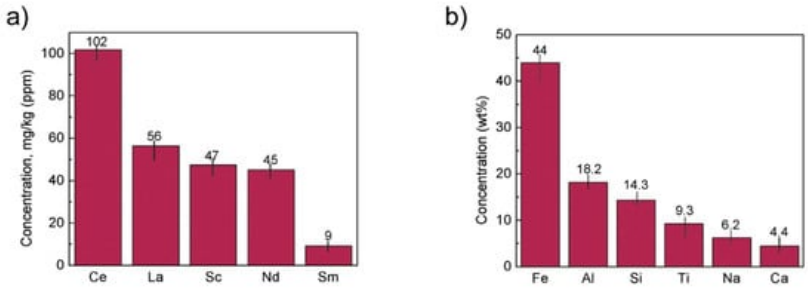

Figure 16. (**a**) REE concentration; (**b**) major element concentration from ICP-OES and XRD elemental composition obtained from red mud. Reprinted from ref. [90].

Lightweight alloys for the transportation industry are in serious demand due to their unique and desired properties as alloys. Bauxite residue is considered as a source hub for these alloys with metals with considerable Ti and Sc contents. The combination of hydrogen peroxide (H_2O_2) and sulfuric acid (H_2SO_4) is used for leaching solution at 90 °C for 30 min to extract Sc and Ti of 68% and 91%, respectively (**Figure 17**).

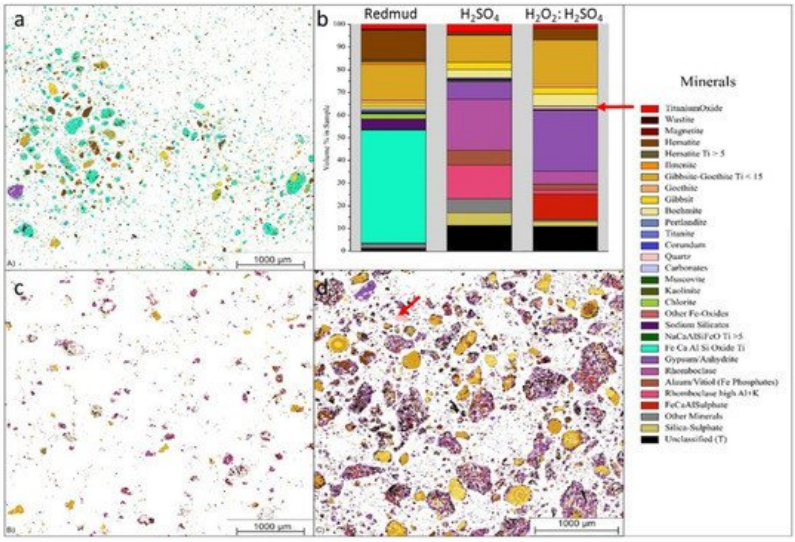

Figure 17. Visual representation of (**a**) the mineralogical distribution of BR; (**b**) phase distribution before and after leaching; (**c**) mineralogical distribution of the leach residue after leaching with 2.5 M H_2SO_4; and (**d**) mineralogical distribution of the leach residue after leaching with 2.5 M H_2SO_4:2.5 M H_2O_2 with S/L = 1/10 at 75 °C for 2 h. Reprinted from ref. [91].

Figure 17 displays the three different minerals (red mud, red mud + H_2SO_4, Red mud + H_2O_2:H_2SO_4) that revealed a very distinct distribution within three samples. Red mud shows the presence of Fe, Ca, Al, and Si oxide with high non-stoichiometric intergrowth oxides. When H_2SO_4 is incorporated, only Si mineral is detected in addition to others, with almost all Fe in leach residue extract as rhomoclase phase [91][92][93]. On incorporating H_2O_2:H_2SO_4 leaching solution, the quartz phase is mostly affected with increasing leaching efficiency. There are inhomogeneous particles with particle sizes ranging from 1 µm to 40 µm. Most of the rare earth particles are based on the Fe-based compositions in combination with Ca, Na, Ti (Fe) O compounds [94][95]. However, the minor elements are based on the C, P, Mn also present in the red mud resources **Figure 17**a,b. **Figure 17**b represents aggregates of the globular region within the red mud particles that may be caused by a cluster of rare earth elements in the reactive combined stage.

The leaching process is one of the effective ways to extract Ti and Fe from the mineralogical sample. The leaching solution of the sulfuric acid and hydrochloric acid is commonly approved for the extraction process [96]. The 67% extraction of Ti from red mud with H_2SO_4 could be achieved by the leaching process [97]. Ti and Fe have different reaction processes in the leaching mechanism for the extraction within the solvent of H_2SO_4 and HCl at different rates. The mechanism of the process is represented in **Figure 18**.

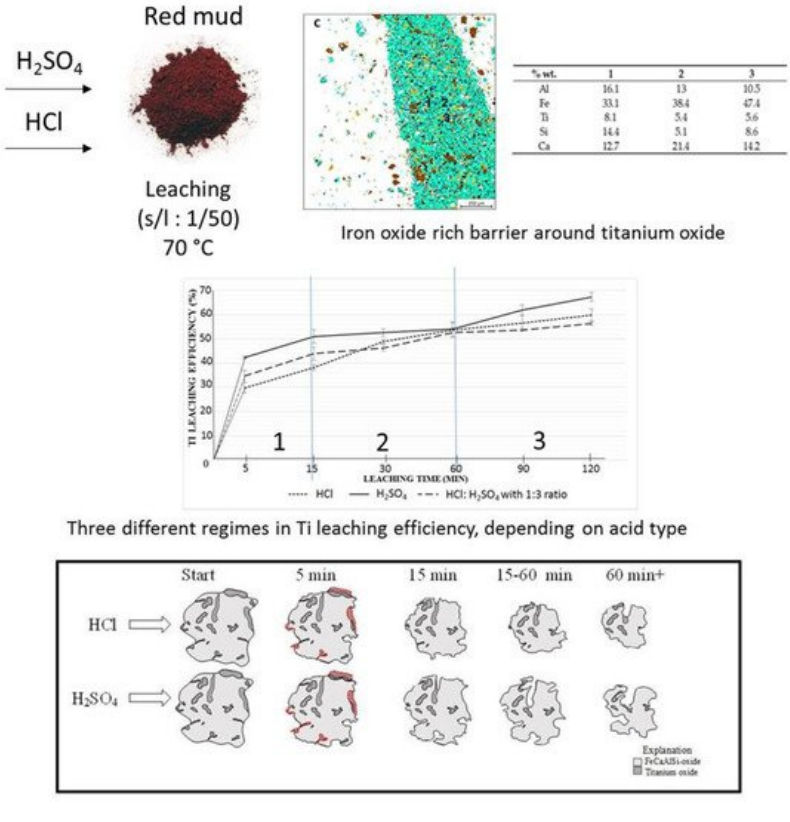

Figure 18. Mineral distribution of red mud shows the presence of various elements and the leaching behavior at various leaching solution and the reacting particle with HCL and H_2SO_4 solution as the function of time. Reprinted from ref. [96].

5. Discussion

Red mud contains various sources of elements in the category of major, minor, and rare earth elements. In the past 11 years, researchers have been more motivated towards the valuable recovery of metal ions from red mud as resources. Although the primary use of red mud is based on the areas of construction sectors [2][12][13][17][18][19][20][39][41][69][70][71], the most valuable secondary concern still arises in the field of metal and mineral sectors. Researchers have focused on various metals present in major and minor quantities in red mud and of which significant amounts could be removed using various processes, such as sintering and carbothermal smelting processes using metallurgical routes [21][22][42][43][44][51][52][53][54][55][56][57][58][59][60][61]. Additional methods, such as the chemical process of leaching, are also investigated as one of the beneficiary ways to extract various categories of elements from red mud [5][18][32][77][86][90][95][96][97][98]. The economic cost of red mud handling and use is one of the important issues associated with the bauxite industry. The general costs of properly handling red mud in some countries are approximately 12 EUR/ton. The general costs of properly handling red mud in various countries are outlined in **Table 3**.

Table 3. General cost of properly handing RM in some countries. Reprinted from ref. [99].

3. Physical and Chemical Properties of Red Mud

3.1. Particle Size Distribution and pH of Red Mud

Red mud, generated as waste in the aluminum industry and generally disposed of in the surrounding areas, was supplied from an Indian bauxite producer (Bharat Aluminium Company Ltd., BALCO, Korba, Chhattisgarh, India). Fly ash was supplied from the thermal power plant (Coal Plant, India). The slurry red mud received directly from the aluminum industry contains a lot of water and moisture. Red mud needs to be dried at 100 °C for 24 h, to remove the water and chemicals such as volatile compounds in a standard furnace in an air medium. The particle sizes of the red mud and pH change as a function of time, as shown in **Figure 5** [53].

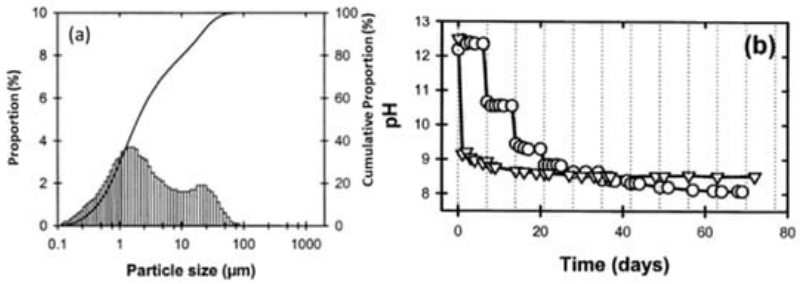

Figure 5. (**a**) Particle size distribution versus cumulative proportion in red mud as the residue from the alumina industry; (**b**) pH as a function of time. Reprint with permission from ref. [53]. Copyright 2004, Wiley.

Red mud consists of various fine-size particles within the range of 0.1–100 μm. Average particles fall within the range of 1 μm. The alkaline nature of red mud decreases as the function of the day, from fresh red mud to aged, and becomes stable. Red mud was mixed with fly ash contents from 0 to 20 Vol% to observe the effect of neutralization of alkaline components with acidic flux by using agate mortar.

3.2. Ternary Phase Diagram of the $CaO–Al_2O_3–SiO_2$ System

Observation of the mineral compounds in the system of the $CaO–Al_2O_3–SiO_2$ phase diagram reveals the red mud–fly ash falling into the category (**Figure 6**).

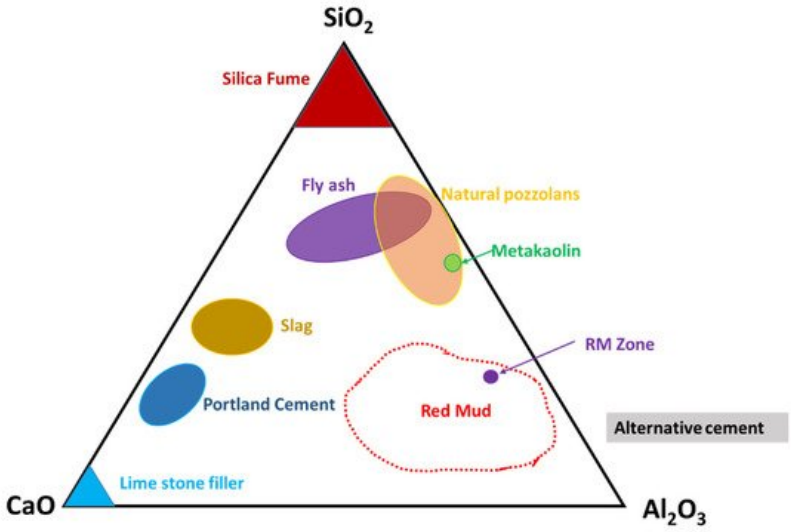

Figure 6. Ternary phase diagram of the $CaO–SiO_2–Al_2O_3$ system that covers red mud and fly ash zones. Reprint with permission from ref. [54]. Copyright 2013, Elsevier.

Thus, their presence in such a diagram could open up the possibility of mixtures of red mud and fly ash for utilization as an alternative cement category for construction purposes. The mixture falls within the zone of slag that could be boosted as a source of metal extraction as well and act as compatible material for alternative cement in the construction industry.

3.3. Phase Transformation during Thermal Decomposition

Differential thermal analysis of red mud showed the combined effect of the decomposition reaction, concerning the weight loss and the associated energy changes. **Figure 7** shows the evolution of red mud as the function of temperature concerning exo- and endothermic reactions [53].

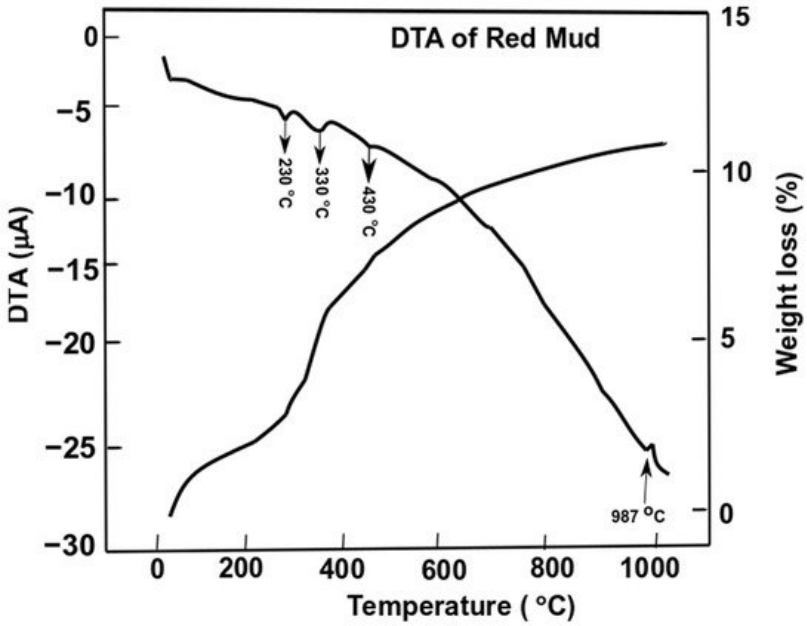

Figure 7. Differential thermal analysis of red mud with peak evolution and weight loss as a function of the temperature. Reprint with permission from ref. [55]. Copyright 2015, Elsevier.

Gibbsite phase emerges between 320 and 330 °C whichderives from the decomposition of $x\text{-}Al_2O_3$. The decomposition reaction of goethite FeO(OH) into hematite and water occurs as follows:

$2\alpha\text{-}FeO(OH)\ (s) \rightarrow Fe_2O_3(s) + H_2O\ (g)$

(1)

whilst the gibbsite decomposes into boehmite and x-alumina in the range of 230–330 °C

$Al(OH)_3\ (s) \rightarrow AlO(OH)\ (s) \uparrow (\text{water evaporates})$

(2)

$2AlO(OH)\ (s) \rightarrow Al_2O_3(s) \uparrow$ (water evaporates)

(3)

Furthermore, goethite continues to decompose into hematite at 440 °C,
$3\ Fe_2O_3\ (s) \rightarrow 2Fe_3O_4\ (s) + ½O_2\ (g)$

(4)

The alumina phase of red mud is very stable until higher temperatures. In the range of 900–1100 °C the formation of nepheline from cancrinite occurs
$3CaO\ (s) + Al_2O_3\ (s) \rightarrow Ca_3Al_2O_6\ (s)$

(5)

and further decomposition reactions happen above 1100 °C
$Fe_2O_3\ (s) \rightarrow 2FeO\ (s) + ½O_2\ (g)$

(6)

$2FeO\ (s) + TiO_2\ (s) \rightarrow Fe_2TiO_4\ (s)$

(7)

$3CaO\ (s) + Fe_2O_3\ (s) + 3\ SiO_2\ (s) \rightarrow Ca_3Fe_2Si_3O_{12}\ (s)$

(8)

$7Ca_3Al_2O_6\ (s) \rightarrow Ca_{12}Al_{14}O_{33}\ (s) + 9CaO\ (s)$

(9)

$Ca_3Al_2O_6\ (s) + Na_2O\ (s) \rightarrow Na_{2x}Ca_{3-x}Al_2O_6\ (s) + xCaO\ (s)$

(10)

The weight loss of the sample of red mud is observed significantly towards higher temperatures. At 1000 °C, there is significant weight loss and more than 10 wt.% loss is observed. DTA analysis reveals the behavior of red mud sintered at a higher temperature.

3.4. Microstructure of Sintered Compound at 1100 °C Temperature

The sintering process further facilitates the mixture as the form of the pellet. Cylindrical pellets were prepared with a dimension of 0.5 × 2.5 cm^2 by using water as a binder at a pressure of 50 MPa. The pellet of red mud–fly ash mixtures with various contents undergoes co-reduction in the graphite resistance furnace for sintering at various temperatures, 1000–1050–1100 °C, for a duration of 2 h in a static argon atmosphere, followed by cooling (2 h).

In **Figure 6**, the microstructure evolution of as-received red mud in dry condition and sintered samples are presented. Globular particles, with fine size in a range from a few microns to the maximum particle size of 100 µm, are displayed (**Figure 8**a). The sintered composite of red mud-fly ash at the various wt.% shows the evolution of various phases as the function of temperature (**Figure 8**b–d). Iron phases of magnetite are shown in a lighter color and the darker region belongs to the quartz. Whereas, sintered red mud–fly ash composite shows isolated pores, elongated shape, and size of the crystals and ceramic matrix with some former phases. The sintered sample with 20 wt.% of fly ash shows that the porosity in sintered composite increased with irregular (Fe_3O_4), goethite (FeO(OH)), iron (Fe), hercynite ($FeAl_2O_4$), and aluminum silicates. Additionally, 20 wt.% of fly ash and sintering at various temperatures allows conversion of complex phases towards simpler phases of compounds of magnetite, iron, calcium aluminosilicate, sodium aluminum silicates, and Goethite phases [55][56].

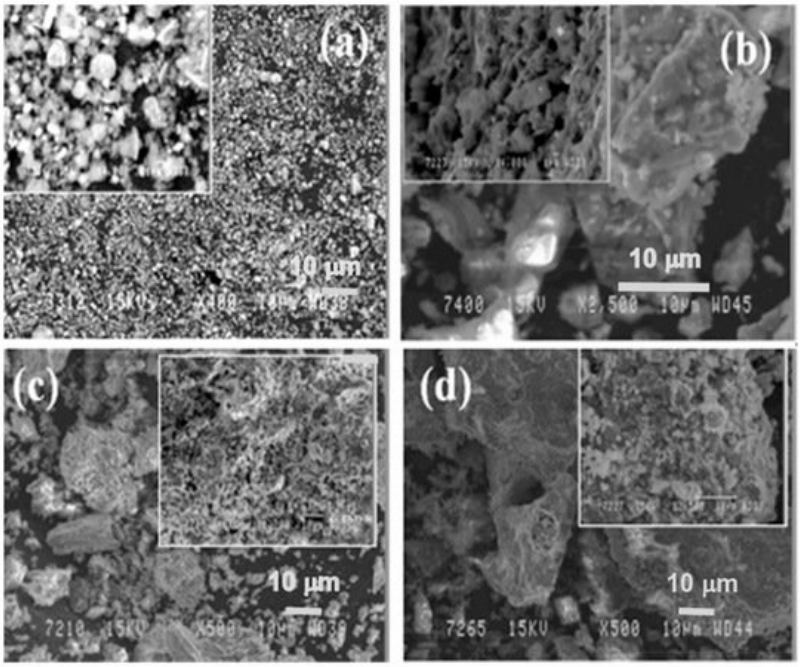

Figure 8. (**a**) Surface features of the red mud at RT; (**b**) sintered red mud without fly ash content; (**c**) sintered red mud with 10 wt.% of fly ash content; (**d**) sintered red mud with 20 wt.% of fly ash content at 1100 °C sintered temperature. Reprint with permission from ref. [55]. Copyright 2015, Elsevier.

3.5. Phase Evolution of Sintered Sample as a Function of Temperature

Figure 9 displays the various phases of magnetite, calcium aluminum silicate, sodium aluminum silicate, goethite, iron, and perovskite as a function of sintering temperature. The phases show a trending behavior with fly ash mixtures of 10 wt.% (**Figure 9**a,b). On increasing the percentage of fly ash content (up to 20 wt.%) phase evolution is more stable and distinct (**Figure 9**c). Metal ions into the various phases are more prominent at lower sintering temperatures without the addition of fly ash [57][58][59]. However, the phases are more distinct and accurate with more specific phases of simpler compounds at a higher sintering temperature of 1100 °C with 20 wt.% of fly ash content. The reduced sintered slag contains various metal ions and mineral sources for the recovery of metal and ions for further utilization in industry [60][61][62].

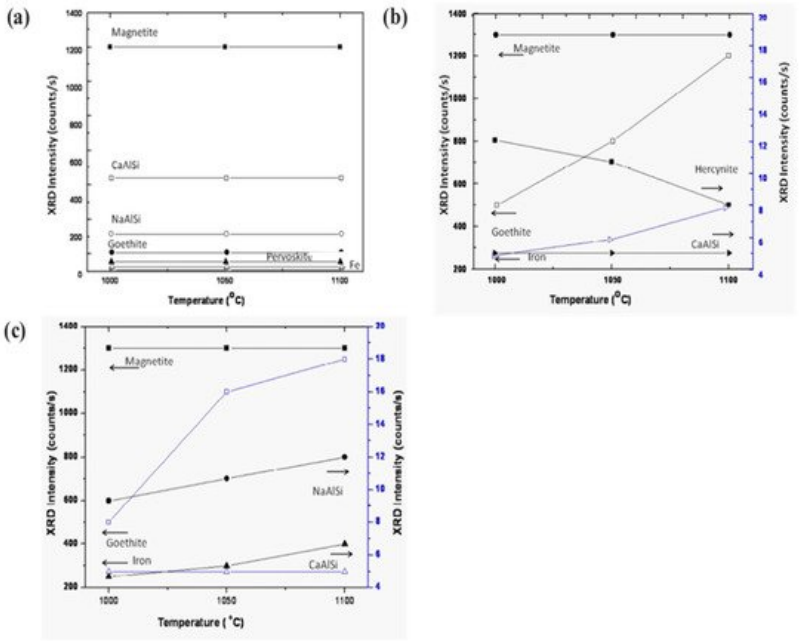

Figure 9. Evolution of various compounds as the function of sintering temperature: (**a**) sintered red mud without any additives; (**b**) sintered red mud with 10 wt.% of fly ash content; (**c**) sintered red mud + 20 wt.% fly ash mixture. Reprint with permission from ref. [55]. Copyright 2015, Elsevier.

3.6. Carbo-Thermal Smelting Technology

Carbo-thermal reduction of bauxite is developing as a promising alternative technology for the aluminum and aluminum alloy industries. In this process, carbon or coke are used as a reductant for solid-state reduction technology. As a result, metallic iron, ferroalloy of silicon and aluminum, titanium carbides could be obtained as the by-products [19][20]. Based on the smelting technology, we performed previous work on using fly ash additive with the red mud that undergoes sintering technology for the building materials. A combination of smelting and reduction processes allows a reduction in the temperature of 1200–1500 °C to produce slag phase and cast iron if the C content in the cast iron is within the range of 2–2.3%. Another direct route for separation of iron from red mud is the roasting method followed by magnetic separation. Iron (Fe) could be separated from red mud using various methods, either by leaching or by sintering or roasting. As one of the major elements, Fe should be extracted from red mud following various reaction, as outlined below [63][64][65].

Fe_2O_3 (s) + C (s) → Fe_3O_4 (s) + CO (g)

(11)

Fe_2O_3 (s) + 3C (s) → Fe (s) + 3CO (g)

(12)

CO_2 (g) + C (s) → 2CO (g)

(13)

$3Fe_2O_3$ (s) + CO (g) → $2Fe_3O_4$ (s) + CO_2 (g)

(14)

Fe_3O_4 (s) + CO (g) → 3FeO (s) + CO_2 (g)

(15)

FeO (s) + CO (g) → Fe (s) + CO_2 (g)

(16)

FeO (s) + C(s) → Fe (s) + CO (g)

(17)

The phases were more prominent in the reduced sample of red mud when 20 wt.% of fly ash was used, which is shown in the SEM images reported in **Figure 10**.

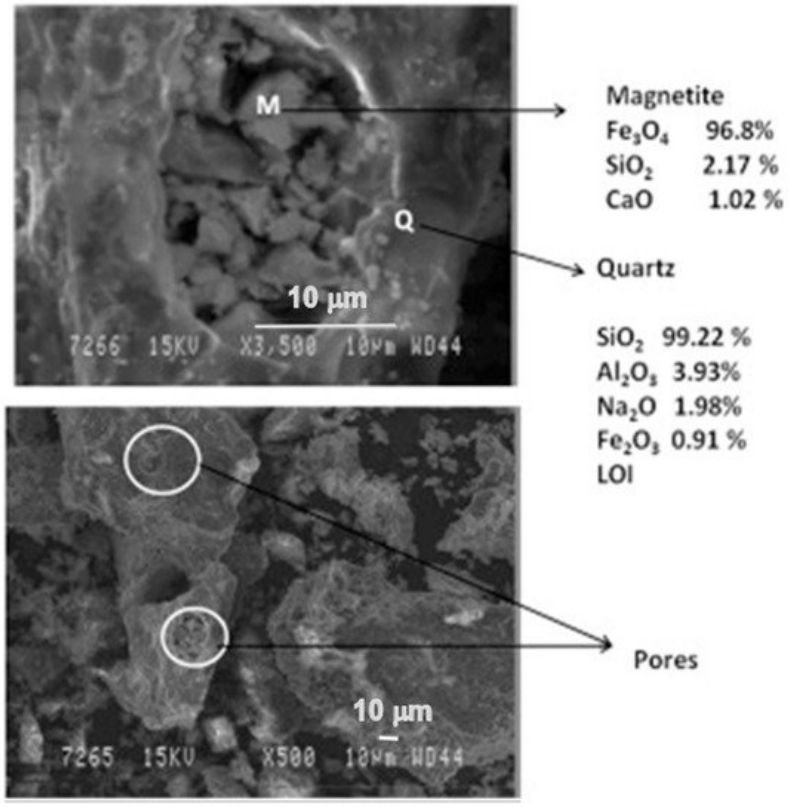

Figure 10. Micrograph of the sintered red mud with 20 wt.% of fly ash content in 1100 °C sintered temperature. Reprint with permission from ref. [55]. Copyright 2015, Elsevier.

The evolution of the different phases developed in the reduced sample sintered up to 1100 °C was recorded with the XRD technique and is shown in **Figure 11**.

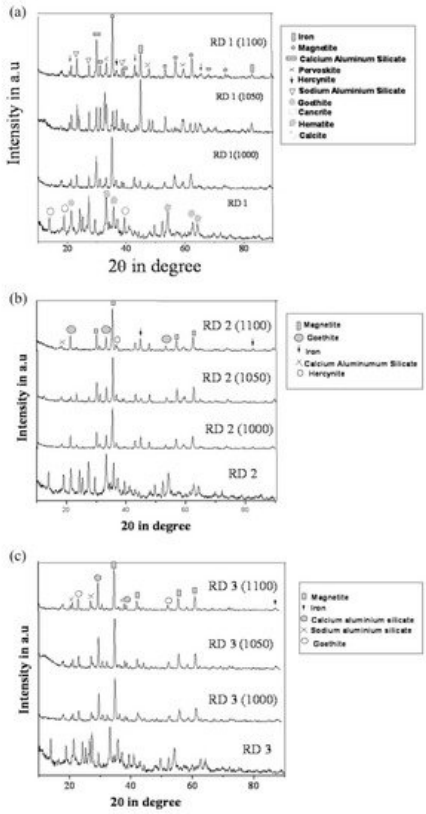

Figure 11. (**a**) Diffraction profile of red mud and sintered red mud at various temperatures; (**b**) diffraction profile of red mud and sintered red mud with 10 wt.% fly ash; and (**c**) diffraction profile of red mud and sintered red mud with 20 wt.% of fly ash content. Reprint with permission from ref. [55]. Copyright 2015, Elsevier.

Iron is the major element in red mud that could directly reduce the carbon-bearing pellets of red mud with coal at a temperature of 1400 °C for 30 min [66]. The obtained products contain 96.52% iron with low Mn and Si contents. However, P and S contents are high.

4. Fields of Application of Red Mud

A considerable environmental concern associated with red mud is associated with its high pH value and its small amounts of heavy metals. These days, the aluminum industries are more focused on producing a cleaner residue from bauxite.

4.1. Thermal Plasma Technology for the Production of By-Products from Red Mud

The thermal plasma technology boom, as a prospective area of waste management, is widely reported in the literature and could be used as a technology to reduce the amount of red mud to produce pig iron [67][68][69]. Red mud mixed with carbon graphite undergoes a smelting process to produce pig iron with 71% recovery. This process allows for reduced energy consumption with recovery of metals from the red mud. Waste treatment is considered one of the efficient methods in the energy sector and thermal power plants. Simultaneously, pig iron could be extracted from red mud by adding a fluxing agent of graphite and fluxes [70][71][72].

4.2. Mixing Technology for Use of Red Mud as an Additive for Construction Materials

Mixing technology is a methodological way of approaching red mud as an alternative replacement of cement. Partially, red mud can be used in slag for the cementitious material that can be used effectively in building sectors [73][74][75]. Red mud is also considered to add a neutralization effect of the hydration properties of cement materials in the construction industry. Bricks and prisms are some of the resources that could be derived from the red-mud-based geopolymer matrix in areas of the building sector. Red mud is considered as environmentally friendly, self-sensing concrete blended with by-product waste. Red mud is also considered as one of the potential additives for durability and mechanical performance of cement mortars. Geopolymerization of red mud and the slag from ferronickel could emerge as advanced inorganic polymeric material with exceptional physical and chemical properties [76][77].

4.3. Separation and Extraction Technology

The separation of the magnetic materials from red mud is considered to be the preliminary step for the separation of iron particles. Simultaneously, extraction technology is more effective in leaching such as chemical technology for the separation of various minerals. The leaching of red mud or sintered red mud is very effective in various sectors for the adsorbents and catalyst categories [78][79][80]. The red mud–fly ash mixtures could be considered as a sustainable acid mine drainage management system. Slag and cement mortar containing non thermally treated dried red mud is considered as opening demand for potential utilization. Red mud is considered an effective additive in geopolymer materials for the adsorption of heavy metal ions.

4.4. Coating Technology

Coating technology opens the door for applications in pigment areas using Ti as pigment ion. Red mud could be used as a coating by thermal plasma spray technologies for wear resistance coating or corrosive resistance coating layers that could stand as a barrier against environmental conditions [81][82][83]. Coatings based on red mud offer an important erosion wear resistance, which can further be improved. Red mud could act as deposition material for surface modification technologies in the plating, diffusion process, surface hardening, and thin-film coating sectors. The red mud–polyester composite coating could act as neutron shielding materials from injurious effects of radiation [84][85][86], thus representing an innovative application of red mud in the industrial sector.

Red mud has emerged as a significant contribution to the hybrid composite. Red mud can be used as a resource for transferring a waste-management approach with natural fibers. A hybrid composite concept has been developed for the potential in a red-mud-based geopolymer matrix with the incorporation of fibers [87].

4.5. Economic and Social Impact

The potential application of red mud in the various industrial sectors proves that valuable resources will have a significant impact on the economic prospects, boosting economic growth through its potential as a valuable by-product. The social impact will increase only by using it as a resource rather than dumping as waste that holds a threat for environmental pollution [88][89][90]. The significant use of red mud as a resource will reduce the risk of environmental hazards and socially benefit environmental conditions.

4.6. Value Recovery and Strategic Utilization

The valuable elements in red mud can be recovered by acid leaching, solid-state carbo-thermic reduction, magnetic and fluidized bed separation, as well as smelting in a blast furnace. In the framework of considering red mud as a resource, we need to improve various steps of metal recovery as one of the potential applications for the pigment industries.

The elemental composition and its derivation from red mud, bauxite residue, and their respective Raman spectra for various elements are shown in **Figure 12** [91]. A red mud image scan analysis shows minerals and ions present in the sample (**Figure 12**) [92].

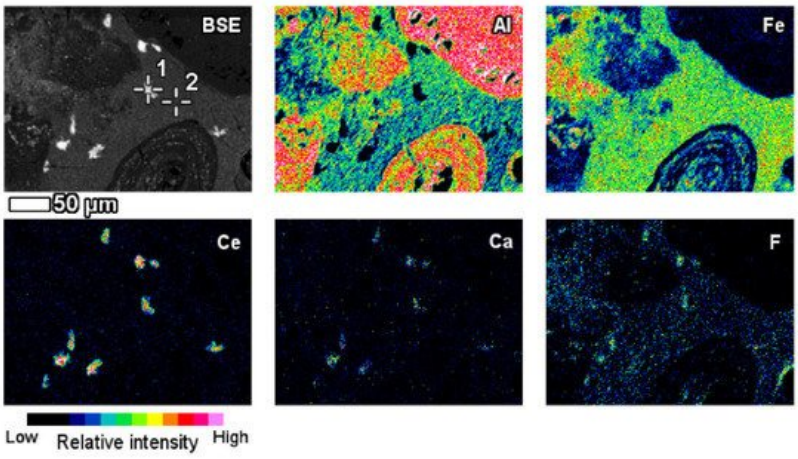

Figure 12. Backscattered image of red mud and elemental image analysis for various elements of Al, Fe, Ce, Ca, F. Reprinted from ref. [91].

An insight investigation was carried out on various phases of rare earth elements in red mud. This approach leads to a mineralogical insight view with output to improve the rare earth elements recovery process. The distinct rare earth element (REE) phases are also contained within the lateritic bauxite (**Figure 12**).

The REE mineral content includes aluminum, cerium, phosphorous, and then other REEs. Thus, REE phases can be identified as belonging to the florencite group. The compositional analysis of elements is done by EDS spectrum exhibiting a pronounced phosphorus X-ray peak of **Figure 13**.

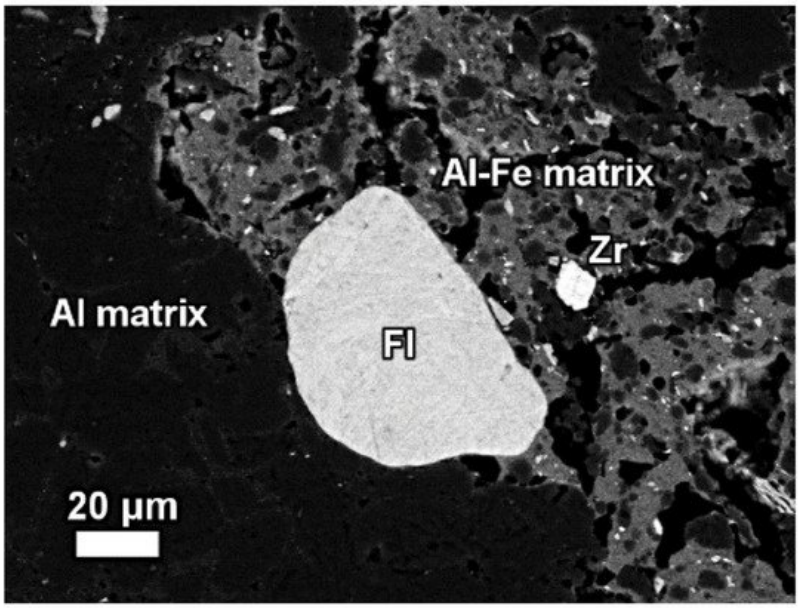

Figure 13. The mineralogical composition of red mud shows the presence of the florencite group of light rare earth elements, grain Zr grain, Al, matrix, and Al–Fe phase. Reprinted from ref. [91].

The composition of grains resembles rhabdophane–Ce which has been detected in the bauxite phase [93]. REE phosphate do not dissolve easily in sodium hydroxide which is generally used in the metal recovery process of bauxite.

LREEs are found as calcium containing phosphate phases in bauxite residue, more specifically as cerium phosphates (**Figure 14**a). It can be seen from the EDS spectrum of an analysed particle, exhibiting a pronounced phosphorus X-ray peak. A wide variation in chemical composition in morphological features is shown in **Figure 14**b.

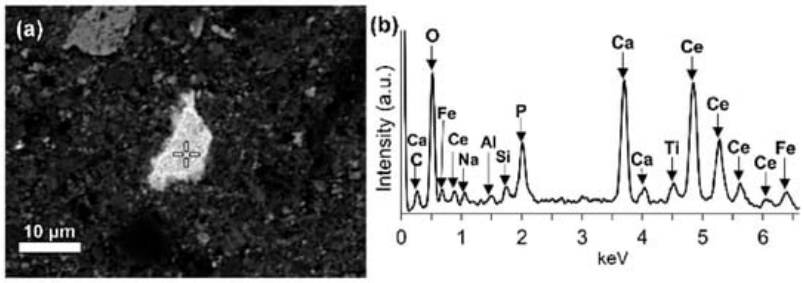

Figure 14. (**a**) Elemental composition of red mud shows the enlarged area of cerium phosphate and (**b**) its respective EDS spectrum. Reprinted from ref. [92].

Some LREE particles contain minor percentages of iron, titanium, and sodium oxide content (**Figure 15**a). The texture of ferrotitanate grains appears anhedral. Others showed distinct zonation expressed in wide variation in chemical composition as well as in morphological features. Most aggregates of anhedral globular crystallites can be observed on examining larger particles that exhibit a different reaction stage that has been observed in **Figure 15**b.

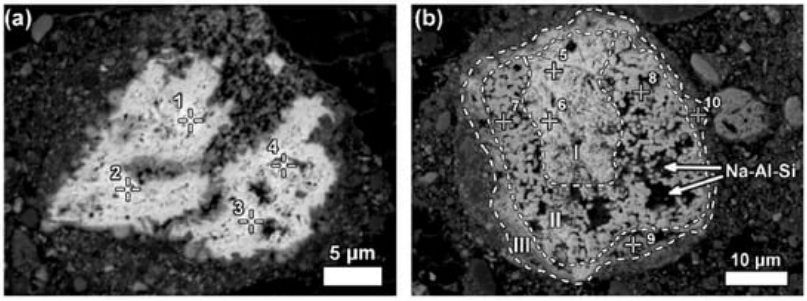

Figure 15. Neodymium–lanthanum as predominant LREE particles, of which (**a**) is partly reacted; and (**b**) exhibits a zonation (I–III) relating to reaction stages with Bayer liquor. Within zone II of (**b**), deposition of a sodium aluminosilicate phase (Na-Al-Si) is indicated. Reprinted from ref. [93].

The concentration of REE elements and major elements from red mud was investigated using ICP-OES and XRD elemental composition (**Figure 16**).

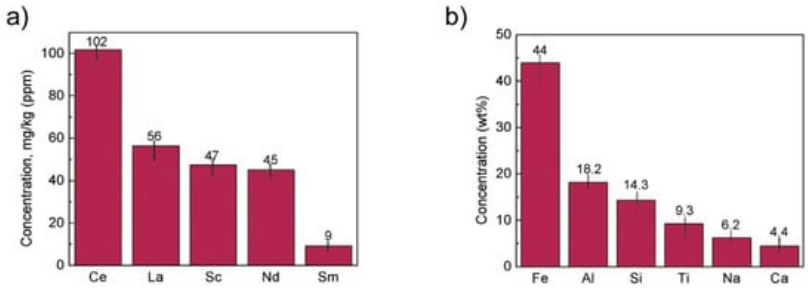

Figure 16. (**a**) REE concentration; (**b**) major element concentration from ICP-OES and XRD elemental composition obtained from red mud. Reprinted from ref. [94].

Lightweight alloys for the transportation industry are in serious demand due to their unique and desired properties as alloys. Bauxite residue is considered as a source hub for these alloys with metals with considerable Ti and Sc contents. The combination of hydrogen peroxide (H_2O_2) and sulfuric acid (H_2SO_4) is used for leaching solution at 90 °C for 30 min to extract Sc and Ti of 68% and 91%, respectively (**Figure 17**).

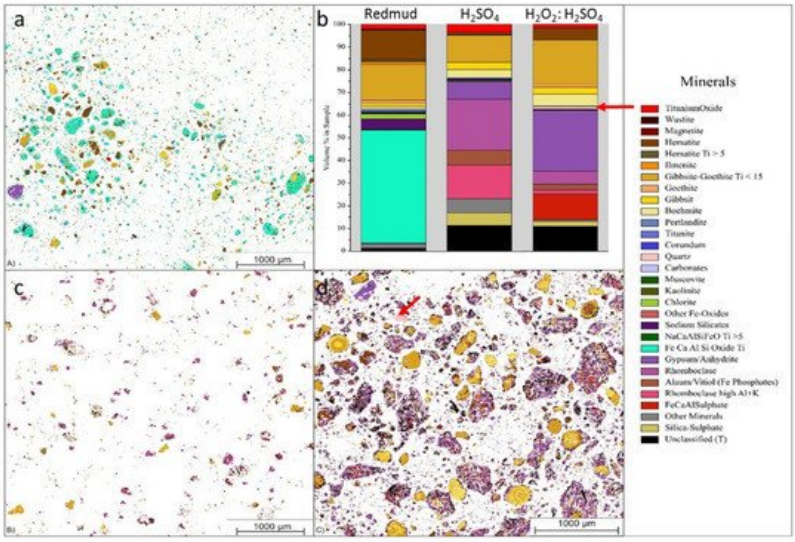

Figure 17. Visual representation of (**a**) the mineralogical distribution of BR; (**b**) phase distribution before and after leaching; (**c**) mineralogical distribution of the leach residue after leaching with 2.5 M H_2SO_4; and (**d**) mineralogical distribution of the leach residue after leaching with 2.5 M H_2SO_4:2.5 M H_2O_2 with S/L = 1/10 at 75 °C for 2 h. Reprinted from ref. [95].

Figure 17 displays the three different minerals (red mud, red mud + H_2SO_4, Red mud + H_2O_2:H_2SO_4) that revealed a very distinct distribution within three samples. Red mud shows the presence of Fe, Ca, Al, and Si oxide with high non-stoichiometric intergrowth oxides. When H_2SO_4 is incorporated, only Si mineral is detected in addition to others, with almost all Fe in leach residue extract as rhomoclase phase [95][96][97]. On incorporating H_2O_2:H_2SO_4 leaching solution, the quartz phase is mostly affected with increasing leaching efficiency. There are inhomogeneous particles with particle sizes ranging from 1 µm to 40 µm. Most of the rare earth particles are based on the Fe-based compositions in combination with Ca, Na, Ti (Fe) O compounds [98][99]. However, the minor elements are based on the C, P, Mn also present in the red mud resources **Figure 17**a,b. **Figure 17**b represents aggregates of the globular region within the red mud particles that may be caused by a cluster of rare earth elements in the reactive combined stage.

The leaching process is one of the effective ways to extract Ti and Fe from the mineralogical sample. The leaching solution of the sulfuric acid and hydrochloric acid is commonly approved for the extraction process [100]. The 67% extraction of Ti from red mud with H_2SO_4 could be achieved by the leaching process [101]. Ti and Fe have different reaction processes in the leaching mechanism for the extraction within the solvent of H_2SO_4 and HCl at different rates. The mechanism of the process is represented in **Figure 18**.

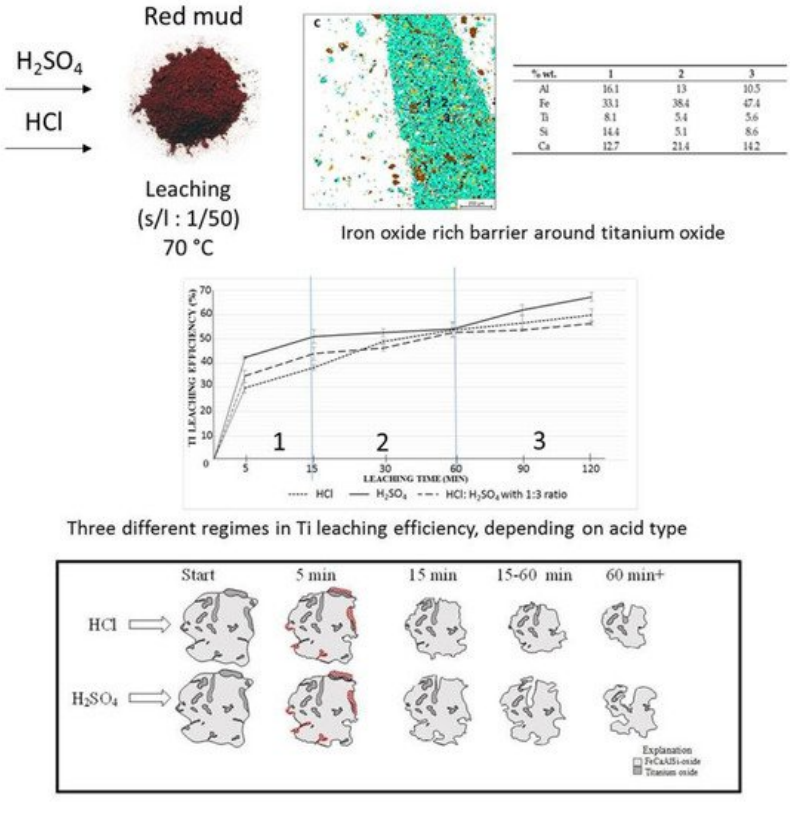

Figure 18. Mineral distribution of red mud shows the presence of various elements and the leaching behavior at various leaching solution and the reacting particle with HCL and H_2SO_4 solution as the function of time. Reprinted from ref. [100].

5. Discussion

Red mud contains various sources of elements in the category of major, minor, and rare earth elements. In the past 11 years, researchers have been more motivated towards the valuable recovery of metal ions from red mud as resources. Although the primary use of red mud is based on the areas of construction sectors [4][5][16][17][21][22][23][24][43][45][73][74][75], the most valuable secondary concern still arises in the field of metal and mineral sectors. Researchers have focused on various metals present in major and minor quantities in red mud and of which significant amounts could be removed using various processes, such as sintering and carbothermal smelting processes using metallurgical routes [25][26][46][47][48][55][56][57][58][59][60][61][62][63][64][65]. Additional methods, such as the chemical process of leaching, are also investigated as one of the beneficiary ways to extract various categories of elements from red mud [9][22][36][81][90][94][99][100][101][102]. The economic cost of red mud handling and use is one of the important issues associated with the bauxite industry. The general costs of properly handling red mud in some countries are approximately 12 EUR/ton. The general costs of properly handling red mud in various countries are outlined in **Table 3**.

Table 3. General cost of properly handing RM in some countries. Reprinted from ref. [103].

The amount of funds will increase by government and industry based on the capacity of alumina production. Nevertheless, it is highly beneficial to construct in-house facility for metal extraction that will reduce the expense of transportation of red mud to other location.

6. Conclusions

A unique cost-effective and environmentally sustainable technique is very challenging to achieve. The recovery of metals and minerals from red mud using multiple different potential techniques need to be emphasized and implemented. Recovery of Fe (44 Wt.%), Al (18.2 Wt.%), Si (14.3 Wt.%), Ti (9.3 Wt.%), Na (6.2 Wt.%), Ca (4.4 Wt.%) as major elements and of Mg, V, Mn, Cr, K as minor elements, and rare earth elements such as Ce (102 mg/kg), La (56 mg/kg), Sc (47 mg/kg), Nd (45 mg/kg), Sm (9 mg/kg) need to be processed from red mud by use of several steps. The establishment of the red mud industry as potential resources on the recovery of metal ions will open up new strategies for the metal industries and pigment sectors. Although a lot of studies have been carried out on the recovery of metals, this step is still very limited to the laboratory scale. The lab-scale approach needs to be enhanced in commercial ways to recover metals from red mud as resources. The development of neutralization of red mud and the extraction of metals from red mud do require a good understanding of chemistry and the reduction process of red mud.

Funding

The work is supported by Operational Programme Research, Development and Education financed by European Structural and Investment Funds and the Czech Ministry of Education, Youth and Sports (Project No. SOLID21-CZ.02.1.01/0.0/0.0/16_019/0000760).

Institutional Review Board Statement

Not applicable.

Informed Consent Statement

Not applicable.

Data Availability Statement

Not applicable.

Conflicts of Interest

The author declares no conflict of interest.

References

1. Rai, S.; Bahadure, S.; Chaddha, M.J.; Agnihotri, A. Disposal Practices and Utilization of Red Mud (Bauxite Residue): A Review in Indian Context and Abroad. *J. Sustain. Metall.* **2020**, *6*, 1. [Google Scholar] [CrossRef]
2. Menzies, N. Seawater Neutralization of Alkaline Bauxite residue and Implications for revegetation. *J. Environ. Qual.* **2004**, *33*, 1877. [Google Scholar] [CrossRef] [PubMed]
3. Yang, Z.; Mocadlo, R.; Zhao, M.; Sisson, R.D., Jr.; Tao, M.; Liang, J. Preparation of a geopolymer from red mud slurry and class F fly ash and its behavior at elevated temperatures. *Constr. Build. Mat.* **2019**, *221*, 308. [Google Scholar] [CrossRef]
4. Samal, S. Effect of high temperature on the microstructural evolution of fiber reinforced geopolymer composite. *Heliyon* **2019**, *5*, e01779. [Google Scholar] [CrossRef]
5. Catauro, M.; Tranquillo, E.; Barrino, F.; Dal Poggetto, G.; Blanco, I.; Cicala, G.; Ognibene, G.; Recca, G. Mechanical and thermal properties of fly ash-filled geopolymers. *J. Therm. Anal. Calorim.* **2019**, *138*, 3267. [Google Scholar] [CrossRef]
6. Samal, S.; Ray, A.K.; Bandopadhyay, A. Proposal for resources, utilization and processes of red mud in India—A review. *Int. J. Miner. Process.* **2013**, *118*, 43. [Google Scholar] [CrossRef]
7. Hammond, K.; Mishra, B.; Apelian, D.; Blanpain, B. CR^3 communication: Red mud—A resource or a waste? *JOM* **2013**, *65*, 340. [Google Scholar] [CrossRef]
8. Tulsidas, H.; Gabriel, S.; Kiegiel, K.; Haneklaus, N. Uranium resources in EU phosphate rock imports. *Resour. Policy* **2019**, *61*, 151–155. [Google Scholar] [CrossRef]
9. Yao, L.; Gao, W.; Ma, X.; Fu, H. Properties Analysis of Asphalt Binders Containing Bayer Red Mud. *Materials* **2020**, *13*, 1122. [Google Scholar] [CrossRef] [PubMed]
10. Borra, C.R.; Pontikes, Y.; Binnemans, K.T.; Gerven, V. Leaching of rare earths from bauxite residue (red mud). *Miner. Eng.* **2015**, *76*, 20–27. [Google Scholar] [CrossRef]
11. Choe, G.; Kang, S.; Kang, H. Mechanical Properties of Concrete Containing Liquefied Red Mud Subjected to Uniaxial Compression Loads. *Materials* **2020**, *13*, 854. [Google Scholar] [CrossRef] [PubMed]
12. Ortega, J.M.; Cabeza, M.; Tenza-Abril, A.J.; Real-Herraiz, T.; Climent, M.Á.; Sánchez, I. Effects of Red Mud Addition in the Microstructure, Durability and Mechanical Performance of Cement Mortars. *Appl. Sci.* **2019**, *9*, 984. [Google Scholar] [CrossRef]
13. Wang, P.; Liu, D.-Y. Physical and Chemical Properties of Sintering Red Mud and Bayer Red Mud and the Implications for Beneficial Utilization. *Materials* **2012**, *5*, 1800–1810. [Google Scholar] [CrossRef]
14. Choe, G.; Kang, S.; Kang, H. Characterization of Slag Cement Mortar Containing Nonthermally Treated Dried Red Mud. *Appl. Sci.* **2019**, *9*, 2510. [Google Scholar] [CrossRef]
15. Rao, P.P. The characteristics and genesis discussion of fracture in dry red mud disposal yard. *Ind. Const.* **2010**, *40*, 73–77. [Google Scholar]
16. Chen, X.; Guo, Y.; Ding, S.; Zhang, H.; Xia, F.; Wang, J.; Zhou, M. Utilization of red mud in geopolymer-based previous concrete with function of adsorption of heavy metal ions. *J. Clean. Prod.* **2019**, *207*, 789. [Google Scholar] [CrossRef]
17. Ascensao, G.; Seabra, M.P.; Aguiar, B.J. Labrincha. J.A. Red mud-based geopolymers with tailored alkali diffusion properties and pH buffering ability. *J. Clean. Prod.* **2017**, *148*, 23. [Google Scholar] [CrossRef]
18. Mahinroosta, M.; Karimi, Z.; Allahverdi, A. Recycling of red mud for value-added applications: A comprehensive Review. *Encyl. Renew. Sust. Mat.* **2020**, *2*, 561. [Google Scholar]
19. Guo, Y.-H.; Gao, J.-J.; Xu, H.-J.; Zhao, K.; Shi, X.-F. Nuggets production by direct reduction of high Iron red mud. *J. Iron Steel Res. Int.* **2013**, *20*, 24–27. [Google Scholar] [CrossRef]
20. Kumar, R.; Srivastava, J.; Premchand, P. Utilization of iron values of red mud for metallurgical applications. *Environ. Waste Manag.* **1998**, 108–119. Available online: https://core.ac.uk/download/pdf/297716085.pdf (accessed on 10 April 2021).
21. Kumar, S.; Kumar, R.; Bandopadhyay, A. Innovative methodologies for the utilization of wastes from metallurgical and allied industries. *Resour. Conserv. Recycl.* **2006**, *48*, 301–314. [Google Scholar] [CrossRef]
22. Jayasankar, K.; Ray, P.K.; Chaubey, A.K.; Padhi, A.; Satapathy, B.K.; Mukherjee, P.S. Production of pig iron from red mud waste fines using thermal plasma technology. *Int. J. Miner. Metall. Mater.* **2012**, *19*, 679–684. [Google Scholar] [CrossRef]
23. Lim, K.; Shon, B. Metal Components (Fe, Al and Ti) recovery from red mud by sulfuric acid leaching assisted with ultrasonic waves. *Int. J. Emerg. Technol. Adv. Eng.* **2015**, *5*, 25–32. [Google Scholar]
24. Voßenkaul, D.; Birich, A.; Müller, N.; Stoltz, N.; Friedrich, B. Hydrometallurgical processing of eudialyte bearing concentrates to recover rare earth elements via low-temperature dry digestion to prevent the silica gel formation. *J. Sustain. Metall.* **2017**, *3*, 79–89. [Google Scholar] [CrossRef]

25. Schwarzenbach, G.; Muehlebach, J.; Mueller, K. Peroxo complexes of titanium. *Inorg. Chem.* **1970**, *9*, 2381–2390. [Google Scholar] [CrossRef]
26. Antonijević, M.; Dimitrijević, M.; Janković, Z. Leaching of pyrite with hydrogen peroxide in sulphuric acid. *Hydrometallurgy* **1997**, *46*, 71–83. [Google Scholar] [CrossRef]
27. Yagmurlu, B.; Dittrich, C.; Friedrich, B. Precipitation Trends of Scandium in Synthetic Red Mud Solutions with Different Precipitation Agents. *J. Sustain. Metall.* **2017**, *3*, 90–98. [Google Scholar] [CrossRef]
28. Khairul, M.A.; Zanganeh, J.; Moghtaderi, B. The composition, recycling and utilisation of bayer red mud. *Resour. Conserv. Recycl.* **2019**, *141*, 483–498. [Google Scholar] [CrossRef]
29. Sutar, H.; Mishra, S.C.; Sahoo, S.K.; Maharana, H. Progress of red mud utilization: An overview. *Am. Chem. Sci. J.* **2014**, *4*, 255–279. [Google Scholar] [CrossRef]
30. Rickhov, V.; Botalov, M.; Kirilov, E.; Kirilov, S.; Semenishchev, V.; Bunkov, G.; Smyshlyaev, D. The investigation of sulphuric acid sorption recovery of scandium and uranium from the red mud of alumina production. *Hydrometallurgy* **1997**, *45*, 249–259. [Google Scholar]
31. Wang, W.; Pranolo, Y.; Cheng, C.Y. Recovery of scandium from synthetic red mud leach solutions by solvent extraction with D2EHPA. *Sep. Purif. Technol.* **2013**, *108*, 96–102. [Google Scholar] [CrossRef]
32. Ning, G.; Zhang, B.; Liu, C.; Li, S.; Ye, Y.; Jiang, M. Large-Scale Consumption and Zero-Waste Recycling Method of Red Mud in Steel Making Process. *Minerals* **2018**, *8*, 102. [Google Scholar] [CrossRef]
33. Pascual, J.; Corpas, F.; López-Beceiro, J.; Benítez-Guerrero, M.; Artiaga, R. Thermal characterization of a Spanish red mud. *J. Therm. Anal. Calorim.* **2009**, *96*, 407–412. [Google Scholar] [CrossRef]
34. Mauskar, J. *Assessement of Utilization of Industrial Solid Waste in Cement Manufacturing*; Central Pollution Control board: Delhi, India, 2006. [Google Scholar]
35. Pratt, K.C.; Christoverson, V. Hydrogenatation of a model hydrogen-donor system using activated red mud catalyst. *Fuel* **1982**, *61*, 460–462. [Google Scholar] [CrossRef]
36. Halász, J.; Hodos, M.; Hannus, I.; Tasi, G.; Kiricsi, I. Catalytic detoxification of C2-chlorohydrocarbons over iron-containing oxide and zeolite catalysts. *Colloids Surf. A* **2005**, *265*, 171–177. [Google Scholar] [CrossRef]
37. Rivera, R.; Ulenaers, B.; Ounoughene, G.; Binnemans, K.; Gerven, T. Extraction of rare earths from bauxite residue (red mud) by dry digestion followed by water leaching. *Miner. Eng.* **2018**, *119*, 82–92. [Google Scholar] [CrossRef]
38. Koumanova, B.; Drame, M.; Popangelova, M. Phosphate removal from aqueous solutions using red mud wasted in bauxite Bayer's process. *Resour. Conserv. Recy.* **1997**, *19*, 11–20. [Google Scholar] [CrossRef]
39. Pera, J.; Boumaza, R.; Ambroise, J. Development of a pozzolanic pigment from red mud. *Cem. Concr. Res.* **1997**, *27*, 1513–1522. [Google Scholar] [CrossRef]
40. Collazo, A.; Fernández, D.; Izquierdo, M.; Nóvoa, X.R.; Pérez, C. Evaluation of red mud as surface treatment for carbon steel painting. *Prog. Org. Coat.* **2005**, *52*, 351–358. [Google Scholar] [CrossRef]
41. Park, S.J.; Jun, B.R. Improvement of red mud polymer-matrix nanocomposites by red mud surface treatment. *J. Colloid Interface Sci.* **2005**, *284*, 204–209. [Google Scholar] [CrossRef]
42. Chunming, G.; Nanr, Y. Effect of phosphate on the hydration of alkali-activated red mud–slag cementitious material. *Cem. Concr. Res.* **2000**, *30*, 1013–1016. [Google Scholar]
43. Ochsenkuhn, P.M.; Lyberropulu, T.; Ochsenkuhn, K.M.; Parissakis, G. Recovery of lanthanides and yttrium from red mud by selective leaching. *Anal. Chim. Acta* **1996**, *319*, 249–254. [Google Scholar] [CrossRef]
44. Wang, S.; Boyjoo, Y.; Choueib, A.; Zhu, Z.H. Removal of dyes from aqueous solution using fly ash and red mud. *Water Res.* **2005**, *39*, 129–138. [Google Scholar] [CrossRef] [PubMed]
45. Smith, N.J.; Buchanan, V.E.; Oliver, G. The potential application of red mud in the production of castings. *Mater. Sci. Eng. A* **2006**, *420*, 250–253. [Google Scholar] [CrossRef]
46. Li, P.; Miser, D.E.; Rabiei, S.; Yadav, R.T.; Hajaligol, M.R. The removal of carbon monoxide by iron oxide nanoparticles. *Appl. Catal. B* **2003**, *43*, 151–162. [Google Scholar] [CrossRef]
47. Lopez, E.; Soto, B.; Arias, M.; Nunez, A.; Rubinos, D.; Barral, T. Adsorbent properties of red mud and its use for wastewater treatment. *Water Res.* **1998**, *32*, 1314–1322. [Google Scholar] [CrossRef]
48. Altundoğan, H.S.; Altundoğan, S.; Tümen, F.; Bildik, M. Arsenic removal from aqueous solutions by adsorption on red mud. *Waste Manag.* **2000**, *20*, 761–767. [Google Scholar] [CrossRef]
49. Komnitsas, K.; Bartzas, G.; Paspaliaris, I. Efficiency of limestone and red mud barriers: Laboratory column studies. *Miner. Eng.* **2004**, *17*, 183–194. [Google Scholar] [CrossRef]
50. Bertocchi, A.F.; Ghiani, M.; Peretti, R.; Zucca, A. Red mud and fly ash for mine sites contaminated with As, Cd, Cu, Pb and Zn. *J. Hazard. Mater.* **2006**, *134*, 112–119. [Google Scholar] [CrossRef]
51. Genc, H.; Tjell, J.C.; McConchie, D.; Schuiling, O. Adsorption of arsenate from water using neutralized red mud. *Colloid Interface Sci.* **2003**, *264*, 327–334. [Google Scholar] [CrossRef]
52. Yalcin, N.; Sevinc, V. Utilization of bauxite waste in ceramic glazes. *Ceram. Int.* **2000**, *26*, 485–490. [Google Scholar] [CrossRef]

53. Kumar, A.; Kumar, S. Development of paving blocks from synergistic use of red mud and fly ash using geopolymerization. *Constr. Build. Mat.* **2013**, *38*, 865. [Google Scholar] [CrossRef]
54. Chen, X.; Lu, A.; Qu, G. Preparation and characterization of foam ceramics from red mud and fly ash using sodium silicate as foaming agent. *Ceram. Int.* **2013**, *39*, 1923. [Google Scholar] [CrossRef]
55. Samal, S.; Ray, A.K.; Bandopadhyay, A. Characterization and microstructure observation of sintered red mud–fly ash mixtures at various elevated temperatures. *J. Clean. Prod.* **2015**, *101*, 368. [Google Scholar] [CrossRef]
56. Lothenbach, B.; Scrivener, K.; Hooton, R.D. Supplementary cementitious materials. *Cem. Concr. Res.* **2011**, *41*, 1244–1256. [Google Scholar] [CrossRef]
57. Samal, S. Study of Porosity on Titania Slag Obtained by Conventional Sintering and Thermal Plasma Process. *JOM* **2016**, *68*, 3000. [Google Scholar] [CrossRef]
58. Blanco, I.; Cicala, G.; Tosto, C.; Recca, G.; Dal Poggetto, G.; Catauro, M. Kinetic study of the thermal dehydration of fly ash filled Geopolymers. *Macromol. Symp.* **2020**. accepted. [Google Scholar] [CrossRef]
59. Samal, S. High temperature oxidation of Metals. *InTech Open* **2016**, *6*, 101–121. [Google Scholar] [CrossRef]
60. Samal, S. Thermal plasma technology: The prospective future in material processing. *J. Clean. Prod.* **2017**, *142*, 3131. [Google Scholar] [CrossRef]
61. Samal, S. *Thermal Plasma Processing of Materials: High Temperature Applications*; Elsevier: Amsterdam, The Netherlands, 2020. [Google Scholar] [CrossRef]
62. Gomez, E.; Amutha Rani, D.; Cheeseman, C.R.; Deegan, D.; Wise, M.; Boccaccini, A.R. Thermal plasma technology for the treatment of wastes: A critical review. *J. Hazard. Mat.* **2009**, *161*, 614. [Google Scholar] [CrossRef]
63. Xiaoming, L.; Na, Z. Utilization of red mud in cement production: A review. *Waste Manag. Res.* **2011**, *29*, 1053. [Google Scholar] [CrossRef]
64. Sglavo, V.M.; Campostrini, R.; Maurina, S.; Carturan, G.; Monagheddu, M.; Budroni, G.; Cocco, G. Bauxite “red mud” in the ceramic industry. Part 1: Thermal behavior. *J. Eur. Ceram. Soc.* **2000**, *20*, 235. [Google Scholar] [CrossRef]
65. Chen, R.; Cai, G.; Dong, X.; Mi, D.; Puppala, A.J.; Duan, W. Mechanical properties and micro mechanism of loess roadbed filling using by product red mud as a partial alternative. *Constr. Build. Mater.* **2019**, *216*, 188. [Google Scholar] [CrossRef]
66. Alam, S.; Das, S.K.; Rao, B.H. Strength and durability characteristic of alkali activated GGBS stabilized red mud as geo-material. *Constr. Build. Mater.* **2019**, *211*, 932. [Google Scholar] [CrossRef]
67. Samal, S.; Thanh, N.P.; Marvalova, B.; Petrikova, I. Thermal characterization of metakaolin-based geopolymer. *JOM* **2017**, *69*, 2480–2484. [Google Scholar] [CrossRef]
68. Jakob, A.; Stucki, S.; Kuhn, P. Evaporation of hevy-metals during the heat treament of municipal solid waste incinerator fly ash. *Environ. Sci. Technol.* **1995**, *29*, 2429. [Google Scholar] [CrossRef] [PubMed]
69. Tang, W.C.; Wang, Z.; Liu, Y.; Cui, H.Z. Influence of red mud on fresh and hardened properties of self-compacting concrete. *Construct. Build. Mater.* **2018**, *178*, 288. [Google Scholar] [CrossRef]
70. Patel, S.; Pal, B. Current status of industrial waste: Red mud an overview. *Int. J. Latest Technol. Eng. Manag. Appl. Sci.* **2015**, *4*, 1–16. Available online: https://www.ijltemas.in/DigitalLibrary/Vol.4Issue8/01-16.pdf (accessed on 10 April 2021).
71. Xue, S.G.; Zhu, F.; Kong, X.F.; Wu, C.; Huang, L.; Huang, N.; Hartley, W. A review of the characterization and revegetation of bauxite residues (Red mud). *Environ. Sci. Pollut. Res.* **2016**, *23*, 1120. [Google Scholar] [CrossRef]
72. Geng, C.; Liu, J.; Wu, S.; Jia, Y.; Du, B.; Yu, S. Novel method for comprehensive utilization of MSWI fly ash through co-reduction with red mud to prepare crude alloy and cleaned slag. *J. Hazard. Mater.* **2020**, *384*, 121315. [Google Scholar] [CrossRef]
73. Geng, C.; Chen, C.; Shi, X.; Wu, S.; Jia, Y.; Du, B.; Liu, J. Recovery of metals from municipal solid waste incineration fly ash and red mud via a co-reduction process. *Resour. Conserv. Recycl.* **2020**, *154*, 104600. [Google Scholar] [CrossRef]
74. Okada, T.; Tomikawa, H. Efficiencies of metal separation and recovery in ash-melting of municipal solid waste under non-oxidative atmospheres with different reducing abilities. *J. Environ. Manag.* **2016**, *166*, 147. [Google Scholar] [CrossRef] [PubMed]
75. Liu, Y.; Zhao, B.; Tang, Y.; Wan, P.; Chen, Y.; Lv, Z. Recycling of iron from red mud by magnetic separation after co-roasting with pyrite. *Thermochim. Acta* **2014**, *588*, 11. [Google Scholar] [CrossRef]
76. Giannopoulou, I.; Dimas, D.; Maragkos, I.; Panias, D. Utilization of metallurgical solid by-products for the development of inorganic polymeric construction materials. *Glob. NEST J.* **2009**, *11*, 127–136. [Google Scholar]
77. Geng, C.; Wang, H.; Hu, W.; Li, L.; Shi, C. Recovery of iron and copper from copper tailings by coal-based direct reduction and magnetic separation. *J. Iron Steel Res. Int.* **2017**, *24*, 991. [Google Scholar] [CrossRef]
78. Hu, H.; Liu, H.; Zhang, Q.; Zhang, P.; Li, A.; Yao, H.; Naruse, I. Sintering characteristics of CaO-rich municipal solid waste incineration fly ash through the addition of Si/Al-rich ash residues. *J. Mater. Cycles. Waste* **2016**, *18*, 340. [Google Scholar] [CrossRef]

79. Kang, S.; Kang, H.; Lee, B. Effects of Adding Neutralized Red Mud on the Hydration Properties of Cement Paste. *Materials* **2020**, *13*, 4107. [Google Scholar] [CrossRef]
80. Cardenia, C.; Balomenos, E.; Panias, D. Optimization of Microwave Reductive Roasting Process of Bauxite Residue. *Metals* **2020**, *10*, 1083. [Google Scholar] [CrossRef]
81. Keller, V.; Stopić, S.; Xakalashe, B.; Ma, Y.; Ndlovu, S.; Mwewa, B.; Simate, G.S.; Friedrich, B. Effectiveness of Fly Ash and Red Mud as Strategies for Sustainable Acid Mine Drainage Management. *Minerals* **2020**, *10*, 707. [Google Scholar] [CrossRef]
82. Chaikin, L.; Shoppert, A.; Valeev, D.; Loginova, I.; Napol'skikh, J. Concentration of Rare Earth Elements (Sc, Y, La, Ce, Nd, Sm) in Bauxite Residue (Red Mud) Obtained by Water and Alkali Leaching of Bauxite Sintering Dust. *Minerals* **2020**, *10*, 500. [Google Scholar] [CrossRef]
83. Nie, Q.; Li, Y.; Wang, G.; Bai, B. Physicochemical and Microstructural Properties of Red Muds under Acidic and Alkaline Conditions. *Appl. Sci.* **2020**, *10*, 2993. [Google Scholar] [CrossRef]
84. Vigneshwaran, S.; Uthayakumar, M.; Arumugaprabu, V. Potential use of industrial waste-red mud in developing hybrid composites: A waste management approach. *J. Clean. Prod.* **2020**, *276*, 124278. [Google Scholar] [CrossRef]
85. Singh, S.; Aswath, M.U.; Ranganath, R.V. Performance assessment of bricks and prisms: Red mud based geopolymer composite. *J. Build. Eng.* **2020**, *32*, 101462. [Google Scholar] [CrossRef]
86. Liu, D.-Y.; Wu, C.-S. Stockpiling and Comprehensive Utilization of Red Mud Research Progress. *Materials* **2012**, *5*, 1232–1246. [Google Scholar] [CrossRef]
87. Laskou, M.; Andreou, G. Rare earth elements distribution and REE-minerals from the Parnassos–Ghiona bauxite deposits, Greece. In Proceedings of the 7th Biennial SGA Meeting on Mineral Exploration and Sustainable Development, Athens, Greece, 24–28 August 2003; pp. 89–92. [Google Scholar]
88. Samal, S. Effect of shape and size of filler particle on the aggregation and sedimentation behavior of the polymer composite. *Powder Technol.* **2020**, *366*, 43–51. [Google Scholar]
89. Samal, S.; Vlach, J.; Kolinova, M.; Kavan, P. Micro-computed tomography characterization of isotropic filler distribution in magnetorheological elastomeric composites. In *Advanced Processing and Manufacturing Technologies for Nanostructured and Multifunctional Materials III*; The American Ceramic Society: Columbus, OH, USA, 2017. [Google Scholar]
90. Samal, S.; Škodová, M.; Blanco, I. Effects of filler distribution on magnetorheological silicon-based composites. *Materials* **2019**, *12*, 3017. [Google Scholar] [CrossRef]
91. Alkan, G.; Yagmurlu, B.; Cakmakoglu, S.; Hertel, T.; Kaya, S.; Gronen, L.; Stopic, S.; Frierich, B. Novel Approach for Enhanced Scandium and Titanium Leaching Efficiency from Bauxite Residue with Suppressed Silica Gel Formation. *Sci. Rep.* **2018**, *8*, 5676. [Google Scholar] [CrossRef]
92. Vind, J.; Malfliet, A.; Blanpain, B.; Tsakiridis, P.E.; Tkaczyk, A.H.; Vassiliadou, V.; Panias, D. Rare Earth Element Phases in Bauxite Residue. *Minerals* **2018**, *8*, 77. [Google Scholar] [CrossRef]
93. Nie, Q.; Hu, W.; Huang, B.; Shu, X.; He, Q. Synergistic utilization of red mud for flue-gas desulfurization and fly ash based geopolymer preparation. *J. Hazard. Mater.* **2019**, *369*, 503. [Google Scholar] [CrossRef]
94. Kaußen, F.M.; Friedrich, B. Phase characterization and thermochemical simulation of (landfilled) bauxite residue ("red mud") in different alkaline processes optimized for aluminum recovery. *Hydrometallurgy* **2018**, *176*, 49–61. [Google Scholar] [CrossRef]
95. Klauber, C.; Gräfe, M.; Power, G. Bauxite residue issues: II. Options for residue utilization. *Hydrometallurgy* **2011**, *108*, 11–32. [Google Scholar] [CrossRef]
96. Goodenough, K.M.; Wall, F.; Merriman, D. The rare earth elements: Demand, global resources, and challenges for resourcing future generations. *Nat. Resour. Res.* **2018**, *27*, 201–216. [Google Scholar] [CrossRef]
97. Binnemans, K.; Jones, P.T. Rare earths and the balance problem. *J. Sustain. Metall.* **2015**, *1*, 29–38. [Google Scholar] [CrossRef]
98. Konkanov, M.; Salem, T.; Jiao, P.; Niyazbekova, R.; Lajnef, N. Environment-Friendly, Self-Sensing Concrete Blended with Byproduct Wastes. *Sensors* **2020**, *20*, 1925. [Google Scholar] [CrossRef] [PubMed]
99. Reid, S.; Tam, J.; Yang, M.; Azimi, G. Technospheric Mining of Rare Earth Elements from Bauxite Residue (Red Mud): Process Optimization, Kinetic Investigation, and Microwave Pretreatment. *Sci. Rep.* **2017**, *7*, 15252. [Google Scholar] [CrossRef] [PubMed]
100. Samal, S. Preparation of synthetic rutile from pre-treated ilmenite/Ti-rich slag with phenol and resorcinol leaching solutions. *Hydrometallurgy* **2013**, *137*, 8–12. [Google Scholar] [CrossRef]
101. Alkan, G.; Schier, C.; Gronen, L.; Stopic, S.; Friedrich, B. A Mineralogical Assessment on Residues after Acidic Leaching of Bauxite Residue (Red Mud) for Titanium Recovery. *Metals* **2017**, *7*, 458. [Google Scholar] [CrossRef]
102. Sayan, E.; Bayramoglu, M. Statistical modeling of sulfuric acid leaching of TiO_2 from red mud. *Hydrometallurgy* **2004**, *71*, 397–401. [Google Scholar] [CrossRef]

103. Wang, L.; Sun, N.; Tang, H.; Sun, W. A Review on Comprehensive Utilization of Red Mud and Prospect Analysis. *Minerals* **2019**, *9*, 362. [Google Scholar] [CrossRef]

References

1. Kumar, A.; Kumar, S. Development of paving blocks from synergistic use of red mud and fly ash using geopolymerization. Constr. Build. Mat. 2013, 38, 865.
2. Chen, X.; Lu, A.; Qu, G. Preparation and characterization of foam ceramics from red mud and fly ash using sodium silicate as foaming agent. Ceram. Int. 2013, 39, 1923.
3. Samal, S.; Ray, A.K.; Bandopadhyay, A. Characterization and microstructure observation of sintered red mud–fly ash mixtures at various elevated temperatures. J. Clean. Prod. 2015, 101, 368.
4. Lothenbach, B.; Scrivener, K.; Hooton, R.D. Supplementary cementitious materials. Cem. Concr. Res. 2011, 41, 1244–1256.
5. Samal, S. Study of Porosity on Titania Slag Obtained by Conventional Sintering and Thermal Plasma Process. JOM 2016, 68, 3000.
6. Blanco, I.; Cicala, G.; Tosto, C.; Recca, G.; Dal Poggetto, G.; Catauro, M. Kinetic study of the thermal dehydration of fly ash filled Geopolymers. Macromol. Symp. 2020. accepted.
7. Samal, S. High temperature oxidation of Metals. InTech Open 2016, 6, 101–121.
8. Samal, S. Thermal plasma technology: The prospective future in material processing. J. Clean. Prod. 2017, 142, 3131.
9. Samal, S. Thermal Plasma Processing of Materials: High Temperature Applications; Elsevier: Amsterdam, The Netherlands, 2020.
10. Gomez, E.; Amutha Rani, D.; Cheeseman, C.R.; Deegan, D.; Wise, M.; Boccaccini, A.R. Thermal plasma technology for the treatment of wastes: A critical review. J. Hazard. Mat. 2009, 161, 614.
11. Guo, Y.-H.; Gao, J.-J.; Xu, H.-J.; Zhao, K.; Shi, X.-F. Nuggets production by direct reduction of high Iron red mud. J. Iron Steel Res. Int. 2013, 20, 24–27.
12. Kumar, R.; Srivastava, J.; Premchand, P. Utilization of iron values of red mud for metallurgical applications. Environ. Waste Manag. 1998, 108–119. Available online: (accessed on 10 April 2021).
13. Xiaoming, L.; Na, Z. Utilization of red mud in cement production: A review. Waste Manag. Res. 2011, 29, 1053.
14. Sglavo, V.M.; Campostrini, R.; Maurina, S.; Carturan, G.; Monagheddu, M.; Budroni, G.; Cocco, G. Bauxite “red mud” in the ceramic industry. Part 1: Thermal behavior. J. Eur. Ceram. Soc. 2000, 20, 235.
15. Chen, R.; Cai, G.; Dong, X.; Mi, D.; Puppala, A.J.; Duan, W. Mechanical properties and micro mechanism of loess roadbed filling using by product red mud as a partial alternative. Constr. Build. Mater. 2019, 216, 188.
16. Alam, S.; Das, S.K.; Rao, B.H. Strength and durability characteristic of alkali activated GGBS stabilized red mud as geo-material. Constr. Build. Mater. 2019, 211, 932.
17. Samal, S.; Thanh, N.P.; Marvalova, B.; Petrikova, I. Thermal characterization of metakaolin-based geopolymer. JOM 2017, 69, 2480–2484.
18. Jakob, A.; Stucki, S.; Kuhn, P. Evaporation of hevy-metals during the heat treament of municipal solid waste incinerator fly ash. Environ. Sci. Technol. 1995, 29, 2429.
19. Tang, W.C.; Wang, Z.; Liu, Y.; Cui, H.Z. Influence of red mud on fresh and hardened properties of self-compacting concrete. Construct. Build. Mater. 2018, 178, 288.
20. Patel, S.; Pal, B. Current status of industrial waste: Red mud an overview. Int. J. Latest Technol. Eng. Manag. Appl. Sci. 2015, 4, 1–16. Available online: (accessed on 10 April 2021).
21. Xue, S.G.; Zhu, F.; Kong, X.F.; Wu, C.; Huang, L.; Huang, N.; Hartley, W. A review of the characterization and revegetation of bauxite residues (Red mud). Environ. Sci. Pollut. Res. 2016, 23, 1120.
22. Geng, C.; Liu, J.; Wu, S.; Jia, Y.; Du, B.; Yu, S. Novel method for comprehensive utilization of MSWI fly ash through co-reduction with red mud to prepare crude alloy and cleaned slag. J. Hazard. Mater. 2020, 384, 121315.
23. Geng, C.; Chen, C.; Shi, X.; Wu, S.; Jia, Y.; Du, B.; Liu, J. Recovery of metals from municipal solid waste incineration fly ash and red mud via a co-reduction process. Resour. Conserv. Recycl. 2020, 154, 104600.

24. Okada, T.; Tomikawa, H. Efficiencies of metal separation and recovery in ash-melting of municipal solid waste under non-oxidative atmospheres with different reducing abilities. J. Environ. Manag. 2016, 166, 147.

25. Liu, Y.; Zhao, B.; Tang, Y.; Wan, P.; Chen, Y.; Lv, Z. Recycling of iron from red mud by magnetic separation after co-roasting with pyrite. Thermochim. Acta 2014, 588, 11.

26. Giannopoulou, I.; Dimas, D.; Maragkos, I.; Panias, D. Utilization of metallurgical solid by-products for the development of inorganic polymeric construction materials. Glob. NEST J. 2009, 11, 127–136.

27. Geng, C.; Wang, H.; Hu, W.; Li, L.; Shi, C. Recovery of iron and copper from copper tailings by coal-based direct reduction and magnetic separation. J. Iron Steel Res. Int. 2017, 24, 991.

28. Hu, H.; Liu, H.; Zhang, Q.; Zhang, P.; Li, A.; Yao, H.; Naruse, I. Sintering characteristics of CaO-rich municipal solid waste incineration fly ash through the addition of Si/Al-rich ash residues. J. Mater. Cycles. Waste 2016, 18, 340.

29. Kang, S.; Kang, H.; Lee, B. Effects of Adding Neutralized Red Mud on the Hydration Properties of Cement Paste. Materials 2020, 13, 4107.

30. Cardenia, C.; Balomenos, E.; Panias, D. Optimization of Microwave Reductive Roasting Process of Bauxite Residue. Metals 2020, 10, 1083.

31. Keller, V.; Stopić, S.; Xakalashe, B.; Ma, Y.; Ndlovu, S.; Mwewa, B.; Simate, G.S.; Friedrich, B. Effectiveness of Fly Ash and Red Mud as Strategies for Sustainable Acid Mine Drainage Management. Minerals 2020, 10, 707.

32. Chaikin, L.; Shoppert, A.; Valeev, D.; Loginova, I.; Napol'skikh, J. Concentration of Rare Earth Elements (Sc, Y, La, Ce, Nd, Sm) in Bauxite Residue (Red Mud) Obtained by Water and Alkali Leaching of Bauxite Sintering Dust. Minerals 2020, 10, 500.

33. Nie, Q.; Li, Y.; Wang, G.; Bai, B. Physicochemical and Microstructural Properties of Red Muds under Acidic and Alkaline Conditions. Appl. Sci. 2020, 10, 2993.

34. Vigneshwaran, S.; Uthayakumar, M.; Arumugaprabu, V. Potential use of industrial waste-red mud in developing hybrid composites: A waste management approach. J. Clean. Prod. 2020, 276, 124278.

35. Singh, S.; Aswath, M.U.; Ranganath, R.V. Performance assessment of bricks and prisms: Red mud based geopolymer composite. J. Build. Eng. 2020, 32, 101462.

36. Liu, D.-Y.; Wu, C.-S. Stockpiling and Comprehensive Utilization of Red Mud Research Progress. Materials 2012, 5, 1232–1246.

37. Laskou, M.; Andreou, G. Rare earth elements distribution and REE-minerals from the Parnassos–Ghiona bauxite deposits, Greece. In Proceedings of the 7th Biennial SGA Meeting on Mineral Exploration and Sustainable Development, Athens, Greece, 24–28 August 2003; pp. 89–92.

38. Samal, S. Effect of shape and size of filler particle on the aggregation and sedimentation behavior of the polymer composite. Powder Technol. 2020, 366, 43–51.

39. Samal, S.; Vlach, J.; Kolinova, M.; Kavan, P. Micro-computed tomography characterization of isotropic filler distribution in magnetorheological elastomeric composites. In Advanced Processing and Manufacturing Technologies for Nanostructured and Multifunctional Materials III; The American Ceramic Society: Columbus, OH, USA, 2017.

40. Samal, S.; Škodová, M.; Blanco, I. Effects of filler distribution on magnetorheological silicon-based composites. Materials 2019, 12, 3017.

41. Alkan, G.; Yagmurlu, B.; Cakmakoglu, S.; Hertel, T.; Kaya, S.; Gronen, L.; Stopic, S.; Frierich, B. Novel Approach for Enhanced Scandium and Titanium Leaching Efficiency from Bauxite Residue with Suppressed Silica Gel Formation. Sci. Rep. 2018, 8, 5676.

42. Vind, J.; Malfliet, A.; Blanpain, B.; Tsakiridis, P.E.; Tkaczyk, A.H.; Vassiliadou, V.; Panias, D. Rare Earth Element Phases in Bauxite Residue. Minerals 2018, 8, 77.

43. Nie, Q.; Hu, W.; Huang, B.; Shu, X.; He, Q. Synergistic utilization of red mud for flue-gas desulfurization and fly ash based geopolymer preparation. J. Hazard. Mater. 2019, 369, 503.

44. Kaußen, F.M.; Friedrich, B. Phase characterization and thermochemical simulation of (landfilled) bauxite residue ("red mud") in different alkaline processes optimized for aluminum recovery. Hydrometallurgy 2018, 176, 49–61.

45. Klauber, C.; Gräfe, M.; Power, G. Bauxite residue issues: II. Options for residue utilization. Hydrometallurgy 2011, 108, 11–32.

46. Goodenough, K.M.; Wall, F.; Merriman, D. The rare earth elements: Demand, global resources, and challenges for resourcing future generations. Nat. Resour. Res. 2018, 27, 201–216.

47. Binnemans, K.; Jones, P.T. Rare earths and the balance problem. J. Sustain. Metall. 2015, 1, 29–38.

48. Konkanov, M.; Salem, T.; Jiao, P.; Niyazbekova, R.; Lajnef, N. Environment-Friendly, Self-Sensing Concrete Blended with Byproduct Wastes. Sensors 2020, 20, 1925.
49. Reid, S.; Tam, J.; Yang, M.; Azimi, G. Technospheric Mining of Rare Earth Elements from Bauxite Residue (Red Mud): Process Optimization, Kinetic Investigation, and Microwave Pretreatment. Sci. Rep. 2017, 7, 15252.
50. Samal, S. Preparation of synthetic rutile from pre-treated ilmenite/Ti-rich slag with phenol and resorcinol leaching solutions. Hydrometallurgy 2013, 137, 8–12.
51. Alkan, G.; Schier, C.; Gronen, L.; Stopic, S.; Friedrich, B. A Mineralogical Assessment on Residues after Acidic Leaching of Bauxite Residue (Red Mud) for Titanium Recovery. Metals 2017, 7, 458.
52. Samal, S. Effect of high temperature on the microstructural evolution of fiber reinforced geopolymer composite. Heliyon 2019, 5, e01779.
53. Catauro, M.; Tranquillo, E.; Barrino, F.; Dal Poggetto, G.; Blanco, I.; Cicala, G.; Ognibene, G.; Recca, G. Mechanical and thermal properties of fly ash-filled geopolymers. J. Therm. Anal. Calorim. 2019, 138, 3267.
54. Chen, X.; Guo, Y.; Ding, S.; Zhang, H.; Xia, F.; Wang, J.; Zhou, M. Utilization of red mud in geopolymer-based previous concrete with function of adsorption of heavy metal ions. J. Clean. Prod. 2019, 207, 789.
55. Ascensao, G.; Seabra, M.P.; Aguiar, B.J. Labrincha. J.A. Red mud-based geopolymers with tailored alkali diffusion properties and pH buffering ability. J. Clean. Prod. 2017, 148, 23.
56. Kumar, S.; Kumar, R.; Bandopadhyay, A. Innovative methodologies for the utilization of wastes from metallurgical and allied industries. Resour. Conserv. Recycl. 2006, 48, 301–314.
57. Jayasankar, K.; Ray, P.K.; Chaubey, A.K.; Padhi, A.; Satapathy, B.K.; Mukherjee, P.S. Production of pig iron from red mud waste fines using thermal plasma technology. Int. J. Miner. Metall. Mater. 2012, 19, 679–684.
58. Lim, K.; Shon, B. Metal Components (Fe, Al and Ti) recovery from red mud by sulfuric acid leaching assisted with ultrasonic waves. Int. J. Emerg. Technol. Adv. Eng. 2015, 5, 25–32.
59. Voßenkaul, D.; Birich, A.; Müller, N.; Stoltz, N.; Friedrich, B. Hydrometallurgical processing of eudialyte bearing concentrates to recover rare earth elements via low-temperature dry digestion to prevent the silica gel formation. J. Sustain. Metall. 2017, 3, 79–89.
60. Ochsenkuhn, P.M.; Lyberropulu, T.; Ochsenkuhn, K.M.; Parissakis, G. Recovery of lanthanides and yttrium from red mud by selective leaching. Anal. Chim. Acta 1996, 319, 249–254.
61. Smith, N.J.; Buchanan, V.E.; Oliver, G. The potential application of red mud in the production of castings. Mater. Sci. Eng. A 2006, 420, 250–253.
62. Schwarzenbach, G.; Muehlebach, J.; Mueller, K. Peroxo complexes of titanium. Inorg. Chem. 1970, 9, 2381–2390.
63. Antonijević, M.; Dimitrijević, M.; Janković, Z. Leaching of pyrite with hydrogen peroxide in sulphuric acid. Hydrometallurgy 1997, 46, 71–83.
64. Li, P.; Miser, D.E.; Rabiei, S.; Yadav, R.T.; Hajaligol, M.R. The removal of carbon monoxide by iron oxide nanoparticles. Appl. Catal. B 2003, 43, 151–162.
65. Lopez, E.; Soto, B.; Arias, M.; Nunez, A.; Rubinos, D.; Barral, T. Adsorbent properties of red mud and its use for wastewater treatment. Water Res. 1998, 32, 1314–1322.
66. Altundoğan, H.S.; Altundoğan, S.; Tümen, F.; Bildik, M. Arsenic removal from aqueous solutions by adsorption on red mud. Waste Manag. 2000, 20, 761–767.
67. Yao, L.; Gao, W.; Ma, X.; Fu, H. Properties Analysis of Asphalt Binders Containing Bayer Red Mud. Materials 2020, 13, 1122.
68. Halász, J.; Hodos, M.; Hannus, I.; Tasi, G.; Kiricsi, I. Catalytic detoxification of C2-chlorohydrocarbons over iron-containing oxide and zeolite catalysts. Colloids Surf. A 2005, 265, 171–177.
69. Sayan, E.; Bayramoglu, M. Statistical modeling of sulfuric acid leaching of TiO2 from red mud. Hydrometallurgy 2004, 71, 397–401.
70. Wang, L.; Sun, N.; Tang, H.; Sun, W. A Review on Comprehensive Utilization of Red Mud and Prospect Analysis. Minerals 2019, 9, 362.